Joule-Thomson Expansion of Gas-Condensates

A Literature Review

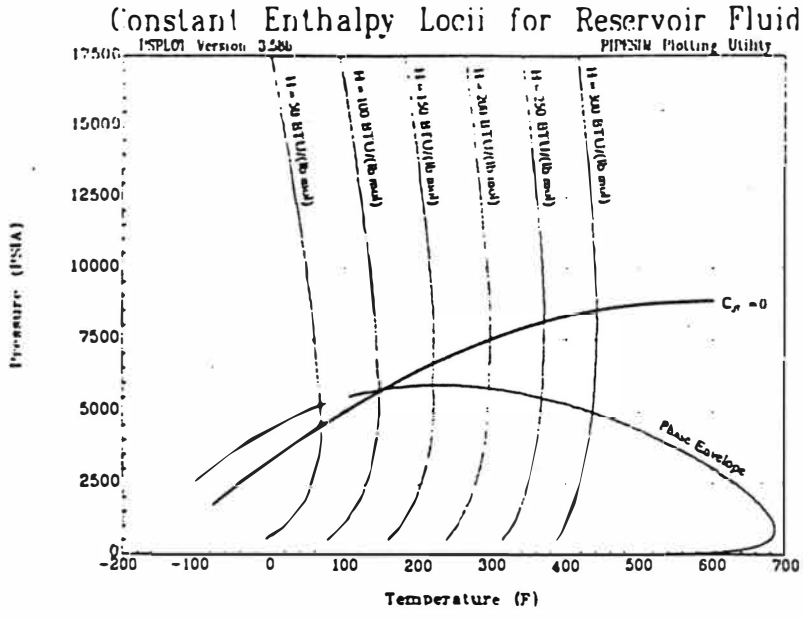

W.G. Kortekaas

November 1994

Supervisors:

Dr. Ir. C.J. Peters
Prof. Dr. Ir. J. de Swaan Arons

Laboratory of Applied Thermodynamics and Phase Equilibria
Faculty of Chemical Technology and Materials Science
Delft University of Technology

Contents

1. Introduction

Recently it was communicated that during gas-condensate production in a North Sea gasfield strong heating of the production stream occurred instead of the expected cooling. This contradictory behaviour called for an investigation of the thermodynamics of these gas-condensate reservoirs. It is expected that due to the high pressure and high temperature conditions in these gas-condensate reservoirs (pressures of approximately 1000 bar and temperatures of 100-200 °C), the Joule-Thomson coefficient will have a negative value and thus heating will take place at expansion; this is called the Joule-Thomson inversion effect. To ensure a safe operation and to ensure that downhole and surface equipment is specified according to downhole temperatures, it is required that pressure and temperature profiles can be accurately estimated for future productions.

The present work is a literature review of what has been reported in the open literature with respect to the Joule-Thomson inversion effect and the heating of gas-condensates at expansion. Chapter 2 will give a general introduction to the Joule-Thomson effect. In chapter 3 the various methods of how to characterize the inversion curve are described and chapter 4 will discuss the calculation of the temperature changes due to expansion. The gas-condensate systems are dealt with in chapter 5 and finally in chapter 6 a summary is given and different aspects, which are important to predict temperature changes for gas-condensate systems, are considered.

2. The Joule-Thomson Effect

2.1 Definition of the Joule-Thomson effect

Figure 2.1 gives a schematic representation of the classical porous plug experiment. The original experiments were first performed by Thomson (later known as lord Kelvin) and Joule in 1853.

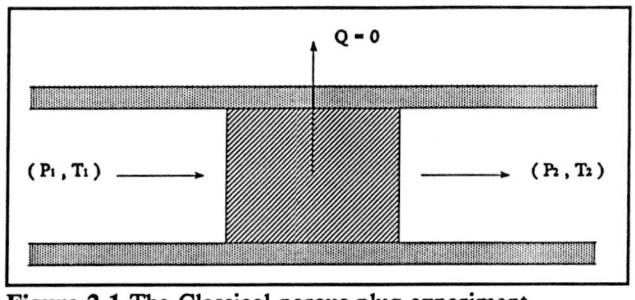

Figure 2.1 The Classical porous plug experiment

In the Joule-Thomson experiment a pressurized fluid, at initial conditions P_1 and T_1, flows under steady state circumstances through a thermally insulated porous plug. The effect of this porous plug is a significant pressure drop across the restriction, causing the fluid to expand. The following energy balance is valid for this system:

$$\Delta H + \frac{1}{2}\Delta v^2 + g\,\Delta z = Q - W \qquad (2.1)$$

Because of steady state flow, it may be assumed that the changes in kinetic energy $\frac{1}{2}\Delta v^2$ and in potential energy $g\Delta z$ are negligible. The plug is fully insulated from the surroundings and therefore the heat effect Q is assumed to be zero. Finally no work W is performed on or by the system and equation 2.1 simply reduces to:

$$\Delta H = 0 \qquad (2.2)$$

and thus the expansion is *isenthalpic*. Such a process for which the inlet and the outlet enthalpy are the same is called *throttling*. Based on the original experiments by Joule and Thomson, the effect of expansion of a fluid from a higher to a lower pressure at constant enthalpy is frequently called the *Joule-Thomson effect*.

When an upstream fluid at pressure P_1 and temperature T_1 crosses the plug the fluid will expand to a downstream pressure P_2 and a temperature T_2. These downstream conditions can

be measured through experimental work. The initial values for P_1 and T_1 are set and the downstream pressure P_2 is varied. For each setting of P_2 the downstream temperature T_2 is then measured. Because the expansion under these conditions is isenthalpic, a set of PT-data is obtained for which the equilibrium states have the same enthalpy. The data can be plotted in a PT-graph and a line of constant enthalpy can be drawn. By choosing new initial values for the pressure P_1, or the temperature T_1, on the upstream side and repeating the experiment, a new line of constant enthalpy is derived. In this manner a whole range of constant-enthalpy lines on a PT-plot can be obtained as shown in figure 2.2.

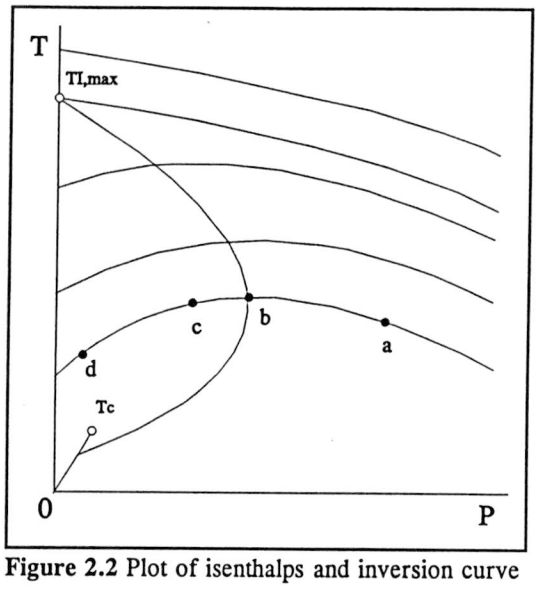

Figure 2.2 Plot of isenthalps and inversion curve

Figure 2.2 shows that throttling of a fluid causes a change in temperature. Depending on de values of P_1, T_1, and P_2 the temperature T_2 after expansion can be higher or lower than the initial temperature. This effect is given by the *Joule-Thomson coefficient* μ_{JT}, which is defined as:

$$\mu_{JT} = \left(\frac{\partial T}{\partial P}\right)_H \qquad \textbf{(2.3)}$$

The Joule-Thomson coefficient is a function of temperature and pressure. In a PT-plot the value of the Joule-Thomson coefficient is represented by the slope of a constant enthalpy line. A number of constant enthalpy lines in figure 2.2 have a state of maximum temperature and in these points the slope and thus the Joule-Thomson coefficient is zero. Values for temperatures where the slope is zero are called *inversion temperatures*. By drawing a line through these inversion temperatures the so-called *inversion curve* is obtained. Because a

given pressure may correspond to two different states, one speaks of an upper and a lower inversion temperature. As can be seen from figure 2.2, a maximum inversion temperature exists (table 2.1) and the inversion curve intersects the vapour pressure line at low temperatures and stops. By extrapolation one can obtain a minimum inversion temperature, which can be convenient but is physically incorrect. Koeppe (1959) showed that the vapour pressure curve can be considered as a prolongation of the inversion curve at low temperatures, though this extended definition of the inversion curve must be accepted with some precaution because the relation $\mu_{JT} = 0$ no longer holds.

The inversion curve is physically very important because it divides the PT-plot into two area's. One for which the μ_{JT} is positive and one for which μ_{JT} is negative (figure 2.3.). The region inside the inversion curve, where the value of μ_{JT} is positive, is called the *cooling region* because a pressure drop causes a decrease in temperature. The region outside the inversion curve, for which μ_{JT} is negative, is called the *heating region* because the temperature increases at pressure drop.

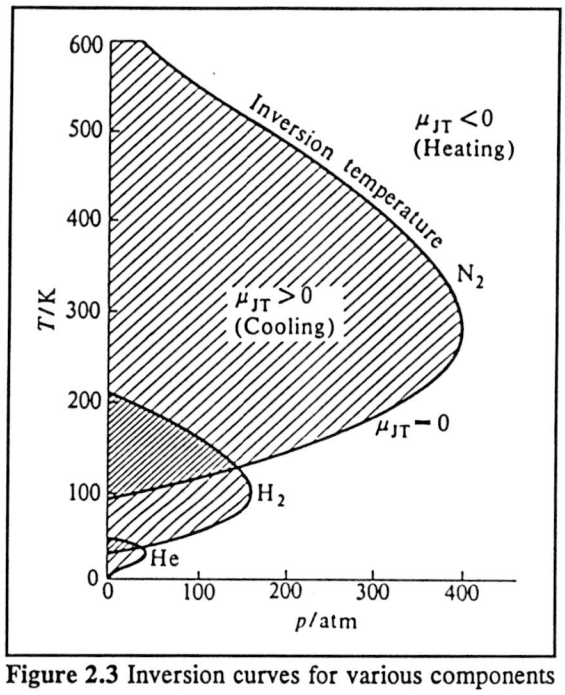

Figure 2.3 Inversion curves for various components

When throttling a fluid, the final temperature may be higher than, equal to, or lower than the initial temperature, depending on the final pressure for any set of initial conditions. For example when a fluid is at an initial state corresponding to point **a** in figure 2.2, expansion to the inversion curve (point **b**) will result in heating of the fluid. When further expansion takes place to point **c** some cooling will occur, but this is not sufficient to lcwer the temperature to that of the initial state. However, if expansion to point **d** is possible, sufficient

cooling will occur to bring the final temperature to a lower value than that of the initial state. Figure 2.2 also shows that for high temperatures enthalpy lines never cross the inversion curve and thus value of the Joule-Thomson coefficient is always negative. At temperatures above this maximum inversion temperature $T_{I,max}$ heating will always occur at expansion. A practical example is the contrasting behaviour of hydrogen and nitrogen at ambient temperature. The maximum inversion temperature of hydrogen, 204 K, is below ambient temperature and, therefore, the negative Joule-Thomson coefficient causes hydrogen to heat at expansion. On the other hand nitrogen has a maximum inversion temperature of 607 K and it is observed that nitrogen cools at expansion.

Table 2.1 Maximum inversion temperatures †

Gas	$T_{I,max}$ (K)
CH_4	939 ‡
CO_2	1275
CO	644
N_2	607
H_2	204
He	43

† Zemansky and Dittman (1981)

‡ Ullmann's (1985)

2.2 The Joule-Thomson coefficient

2.2.1 Experimental work

As mentioned in the previous paragraph, Joule-Thomson experiments began in the 19th century utilizing a porous plug apparatus. The porous plug in these first experiments evolved from a boxwood tube plugged with cotton wool and silk fibre to a fine-grained alundum thimble. With this experimental set-up the first reliable data were produced by Roebuck (1925) for air and other fixed gases (1935, 1942) and by Budenholzer (1939, 1940, 1942), and Sage and Lacey (1936, 1937, 1942) for hydrocarbons. Later Johnston (1949) used a valve arrangement to produce data and it was this valve that was improved and modified by Ahlert (1969). Randelman and Wenzel (1988) used Ahlert's apparatus without significant modification for measuring Joule-Thomson coefficients for mixtures of methane and hydrogen.

In numerous studies Joule-Thomson coefficients have been measured for primarily pure components and the number of these studies by far exceeds the number of investigations

mentioned above. This paragraph merely summarizes the development of experimental work performed on Joule-Thomson coefficients.

2.2.2 Calculation of the Joule-Thomson coefficient

One way to calculate the Joule-Thomson coefficient is by using generalized charts. Edminster (1949) prepared charts and tables for hydrocarbon systems. Joule-Thomson coefficients were calculated for five pure hydrocarbons and eleven hydrocarbon mixtures and the average deviations of this method was 7 percent.

Another possibility is to express the Joule-Thomson coefficient in terms of measurable properties of a fluid. Using the cyclic relation

$$\left(\frac{\partial P}{\partial H}\right)_T \left(\frac{\partial H}{\partial T}\right)_P \left(\frac{\partial T}{\partial P}\right)_H = -1 \qquad \textbf{(2.4)}$$

in equation 2.3 gives:

$$\mu_{JT} = -\frac{1}{C_p}\left(\frac{\partial H}{\partial P}\right)_T \qquad \textbf{(2.5)}$$

For the enthalpy the next generalized equation, given by Smith and van Ness (1987), is used:

$$dH = C_P dT + \left[V - T\left(\frac{\partial V}{\partial T}\right)_P\right] dP \qquad \textbf{(2.6)}$$

By differentiating equation 2.6 with respect to pressure at constant temperature and then substituting into equation 2.5, the following result is obtained:

$$\mu_{JT} = \frac{1}{C_p}\left[T\left(\frac{\partial V}{\partial T}\right)_P - V\right] \qquad \textbf{(2.7)}$$

The Joule-Thomson coefficient can now be calculated from the knowledge of the *PVT* properties of the fluid and the specific heat at constant pressure for that state.

Hirose et al. (1990) presented a paper to estimate the Joule-Thomson coefficients by using equations of state. Calculation of Joule-Thomson coefficients includes differential and integral operations, which can be very complex work.

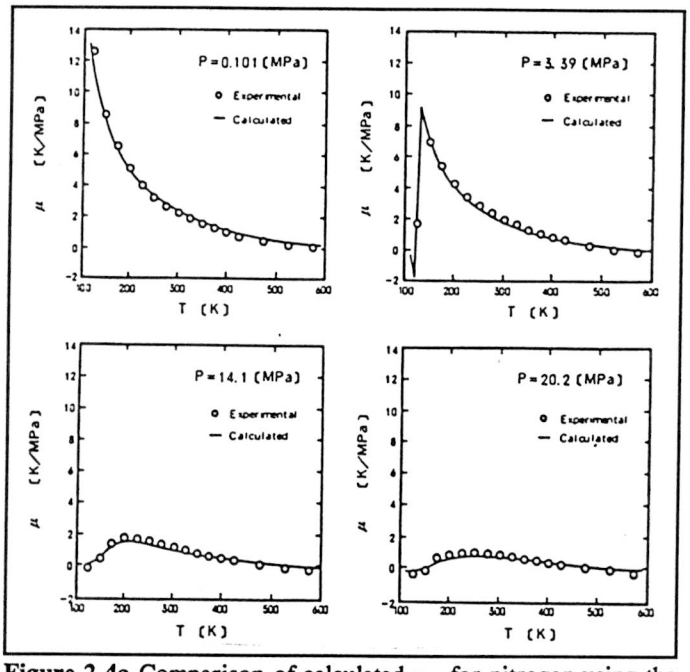

Figure 2.4a Comparison of calculated μ_{JT} for nitrogen using the RK equation with data obtained from the literature (Hirose et al., 1990)

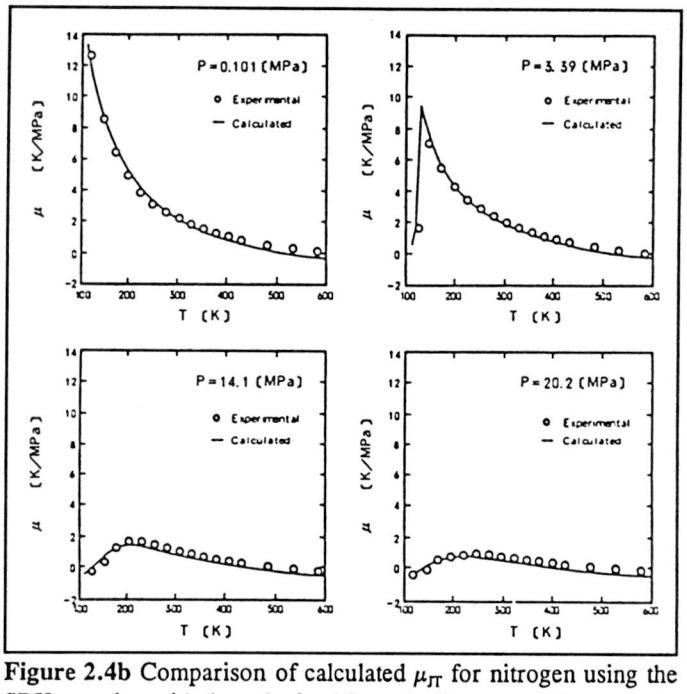

Figure 2.4b Comparison of calculated μ_{JT} for nitrogen using the SRK equation with data obtained from the literature (Hirose et al., 1990)

Therefore they derived practical formulas from various equations of state to calculate the Joule-Thomson coefficients. This was done by use of the Automatic Derivative Derivation System (ADDS). To calculate the specific heat coefficient C_P in equation 2.7 they used the following expressions:

$$C_P = C_P^{id} + (C_P - C_V) + (C_V - C_V^{id}) - R \tag{2.8}$$

$$C_P - C_V = -T\left(\frac{\partial P}{\partial T}\right)_V^2 \left(\frac{\partial P}{\partial V}\right)_T^{-1} \tag{2.9}$$

$$C_V - C_V^{id} = \int_\infty^V T\left(\frac{\partial^2 P}{\partial T^2}\right)_V dV \tag{2.10}$$

Because in general equations of state are not expressed explicit in V, the cyclic relation

$$\left(\frac{\partial V}{\partial T}\right)_P = -\left(\frac{\partial P}{\partial T}\right)_V \left(\frac{\partial P}{\partial V}\right)_T^{-1} \tag{2.11}$$

is used in equation 2.7 and μ_{JT} can be evaluated analytically.
The following five equations of state were studied: **Van der Waals** (VDW), **Virial** (VIR), **Benedict-Webb-Rubin** (BWR), **Redlich-Kwong** (RK) and **Soave-Redlich-Kwong** (SRK). In appendix A the practical formulas produced by the ADDS system for the equations of state are shown. These formulas were used to calculate the values of μ_{JT} for nitrogen and ethane. Figures 2.4a and 2.4b show the calculated results for nitrogen for RK and SRK. The average relative errors (ARE,%) calculated for ethane are shown in table 2.2.

Table 2.2 ARE of μ_{JT} for ethane

EoS	ARE,%	EoS	ARE,%
VDW	1.59	RK	1.07
VIR	25.04	SRK	4.23
BWR	45.45		

From the figures 2.4a and b, and from table 2.2 Hirose et al. (1990) concluded that of these five equations, RK gives the best results for calculating the Joule-Thomson coefficient despite its simple form and the fact that only two critical constants (T_c and P_c) are required. No remarks were made on the influence of the acentric factor ω on calculated results for larger molecules.

3. Characterization of the Joule-Thomson Inversion Curve

Over the years several papers have been published describing the Joule-Thomson inversion effect and the characterization of the Joule-Thomson inversion curve. This chapter describes the various methods that were found in literature to predict the inversion curve for pure components. Also the inversion curve for gas-mixtures will be discussed.

3.1 Inversion curves for pure components

3.1.1 Generalized charts and acentric factor equations

As mentioned in chapter 2 inversion points can be characterized by maxima in H(P) plots or by $\mu_{JT}=0$. Miller (1970) examined several generalized corresponding state charts for enthalpy and μ_{JT}. Because these charts are difficult to read and no values are available above $T_r=4$, these charts have no practical value in characterizing the inversion curve.
Miller also reported that by differentiating the generalized acentric factor equations of Pitzer and Brewer (1961) for enthalpy, an expression can be obtained for $(\partial H/\partial P)_T$. At inversion conditions $(\partial H/\partial P)_T$ is equal to zero and thus the maximum reduced inversion temperature $T_{rI,max}$ as a function of the acentric factor ω is obtained. For $\omega=0$, 0.1 and 0.2 values of 5.14, 4.58 and 4.13 for $T_{rI,max}$ are calculated. Since some gases with $\omega>0$ have experimental values of $T_{rI,max}$ close to 5.0, Pitzer's equation seems to be inadequate.

3.1.2 Correlation of experimental data

A general correlation for the inversion curve can be obtained by a curve fit of inversion points derived from experimental data. Direct measurement of the Joule-Thomson coefficient is difficult because near inversion conditions the temperature change is very small even with large pressure differences. As a result temperature measurements must be extremely accurate to obtain reliable data. In order to obtain Joule-Thomson data, reliable volumetric data are used. This is possible by using the isothermal Joule-Thomson coefficient:

$$\mu_{JT} = \frac{RT^2}{C_P P}\left(\frac{\partial Z}{\partial T}\right)_P = 0 \qquad (3.1)$$

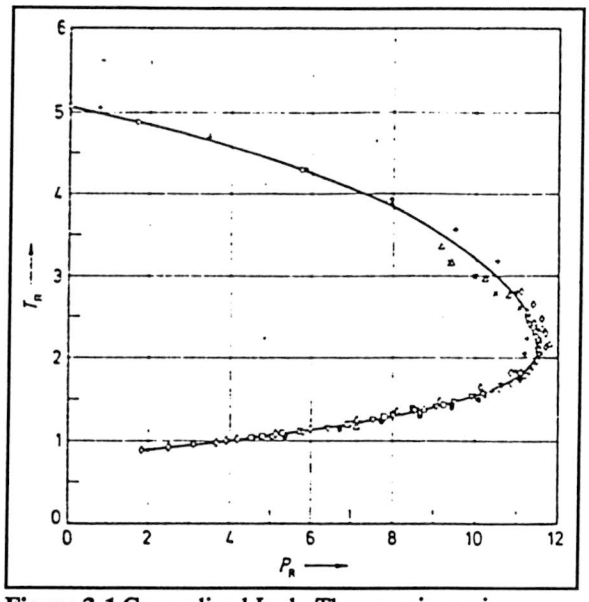

Figure 3.1 Generalized Joule-Thomson inversion curve for cryogenic gases (Gunn et al., 1966)

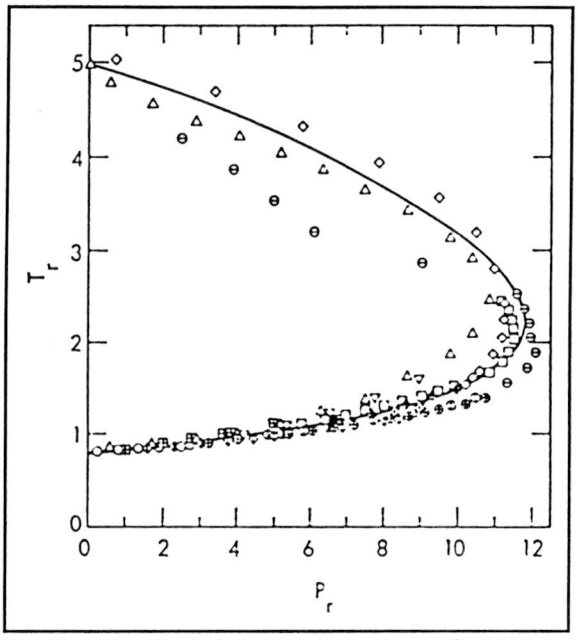

Figure 3.2 Experimental data for points along inversion curve (Miller, 1970)

Since C_p is never zero, the inversion curve can be defined by using the condition $(\partial Z/\partial T)_P=0$. Thus given reliable volumetric data for a gas, it is possible to determine the inversion curve from equation 3.1, be it that the range of temperature and pressure of the available data are sufficiently large.

In the work of Gunn et al. (1966) an estimation of the inversion curve is presented for cryogenic gases. Using previously published, reliable volumetric data for Ar, CO, C_2H_4, CH_4, N_2 and Xe, they calculated inversion points. To obtain an inversion curve that is valid for all gases a plot was made of reduced temperature versus reduced pressure. Using a least-squares fit of the experimental data points, the following correlation was derived (figure 3.1):

$$P_r = -36.275 + 71.598\,T_r - 41.567\,T_r^2 + 11.826\,T_r^3 - 1.6721\,T_r^4 + 0.091167\,T_r^5 \qquad \textbf{(3.2)}$$

Because accurate volumetric data are extremely rare at high reduced temperatures, the upper branch of the curve was based solely on data for carbon monoxide and inversion points determined from theoretical second and third virial coefficients. These were calculated using the Kihara potential for argon. The peak and the lower branch of the curve however are very well defined. Since the substances used in the correlation have acentric factor values close to zero, this correlation is limited to simple fluids.

In the paper presented by Miller (1970) another empirical equation curve is fitted through experimental data. The next three-parameter correlation was obtained by a least squares fit (figure 3.2):

$$P_r = 24.21 - 18.54\,T_r^{-1} - 0.825\,T_r^2 \qquad \textbf{(3.3)}$$

This equation yields a maximum reduced inversion temperature of 4.984 and a lower (extrapolated) inversion temperature of 0.782. This lower temperature is physically incorrect because the lower branch of the inversion curve ends at the vapour pressure curve ($T_r\approx0.8$, $P_r\approx0.3$). The maximum value of the reduced pressure is 11.79 at $T_r=2.24$.

3.1.3 Equations of state

Several studies have been made to compare various equations of state in their ability to predict the inversion curve. The prediction of the inversion curve can be considered as an extreme severe test of an equation of state. To calculate the points of the inversion curve from an equation of state, equation 2.7 has to be altered because equations of state cannot be expressed by V in an explicit form. By using the cyclic relation:

$$\left(\frac{\partial V}{\partial T}\right)_P\left(\frac{\partial T}{\partial P}\right)_V\left(\frac{\partial P}{\partial V}\right)_T = -1 \qquad (3.4)$$

equation 2.7 can be rewritten as:

$$\mu_{JT} = \frac{1}{C_P}\left(-T\left(\frac{\partial P}{\partial T}\right)_V\left(\frac{\partial P}{\partial V}\right)_T^{-1} - V\right) \qquad (3.5)$$

At inversion conditions $\mu_{JT}=0$ and since C_P is never equal to zero, the locus of the inversion points for any equation of state can be calculated by solving the following equation:

$$T\left(\frac{\partial P}{\partial T}\right)_V + V\left(\frac{\partial P}{\partial V}\right)_T = 0 \qquad (3.6)$$

or by transforming into reduced variables:

$$T_r\left(\frac{\partial P_r}{\partial T_r}\right)_{V_r} + V_r\left(\frac{\partial P_r}{\partial V_r}\right)_{T_r} = 0 \qquad (3.7)$$

Juris and Wenzel (1972) reported that prior to 1970 Joule-Thomson inversion curves had only be calculated for the **van der Waals**, the **Dieterici**, the **Lennard-Jones-Devonshire**, and the **DeBoer-Michels** equations of state. This work was done by Corner (1939). Miller (1970) calculated inversion curves for the **Van der Waals, Dieterici, generalized Redlich-Kwong** and **Martin** equations of state, while Juris and Wenzel used the **van der Waals, Dieterici, virial, Berthelot, Redlich-Kwong** (RK), **Beattie-Bridgeman, Benedict-Webb-Rubin** (BWR) and **Martin-Hou** equations of state. In the study of Dilay and Heidemann (1986) four more recent equations of state were tested on their ability to predict the inversion curve: the **Soave-Redlich-Kwong** (SRK), **Peng-Robinson** (PR), **perturbed-hard-chain** (PHC) and **Lee-Kesler** (LK) equations of state. Geană and Feroiu (1992) proposed a **general equation of state** (GEoS) which was compared with the predictions of the SRK, PR and RK equations of state. In this chapter a summary will be given of the most important equations of state used in these previous works and a comparison will be made of the ability of these equations of state to predict the Joule-Thomson inversion curve. All inversion curves predicted by the different equations are compared with the Gunn-Chueh-Prausnitz correlation (eqn. 3.2), for which results are shown in table 3.1. In appendix B expressions for the parameters used in the different equations of state are given.

Table 3.1 Comparison of maximum inversion pressure and temperatures

	Maximum inversion pressure		
	$T_{r,max}$	T_r	$P_{r,max}$
Gunn et al.[a]	5.074	2.174	11.510
Miller[b]	4.98	2.24	11.79
Van der Waals[b]	6.75	3.0	9.0
Dieterici[b]	8.0	4.0	17.93
Berthelot[c]	3.2†	1.5†	8.4†
Redlich-Kwong[b]	5.338	2.21	10.82
Modified RK[d]	5.077	2.0†	11.8†
Soave-Redlich-Kwong[a]	4.141	2.174	11.510
Peng-Robinson[a]	4.977	2.317	13.389
Perturbed-Hard-Chain[a]	4.202	2.257	13.389
Lee-Kesler[a]	4.978	2.303	12.197
GEoS 1[e]	8.2†	2.3†	10.6†
GEoS 2[e]	6.0†	2.2†	11.5†

[a] calculations for simple fluids (ω=0); Dilay and Heidemann (1986)

[b] Miller (1970)

[c] Juris and Wenzel (1972)

[d] Heyes and Llaguno (1992)

[e] calculations for argon; Geană and Feroiu (1992)

† values read from graph

Two-parameter equations of state

Juris and Wenzel (1972) made a comparison between four two-parameter equations of state. In these equations the acentric factor ω is not taken into account. The following equations were used:

Van der Waals:
$$P = \frac{RT}{V-b} - \frac{a}{V^2} \tag{3.8}$$

Dieterici:
$$P = \frac{RT}{V-b} e^{-a/RTV} \tag{3.9}$$

Berthelot:
$$P = \frac{RT}{V-b} - \frac{a}{TV^2} \tag{3.10}$$

Redlich-Kwong:
$$P = \frac{RT}{V-b} - \frac{a}{\sqrt{T}V(V+b)} \tag{3.11}$$

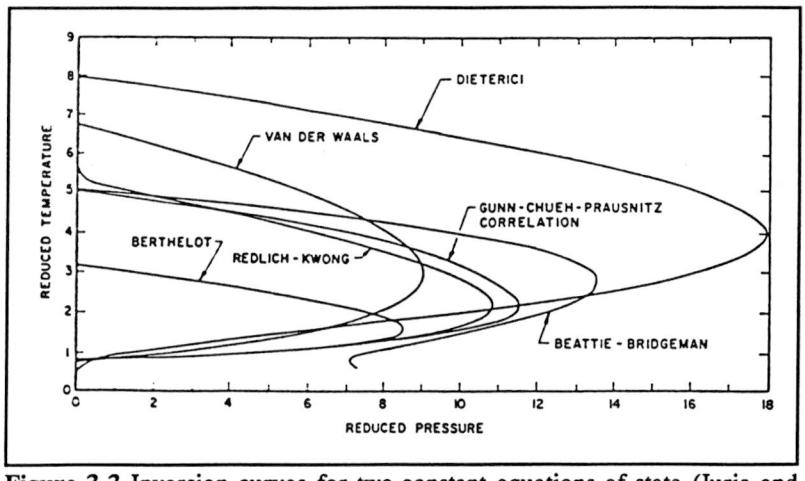

Figure 3.3 Inversion curves for two-constant equations of state (Juris and Wenzel, 1972)

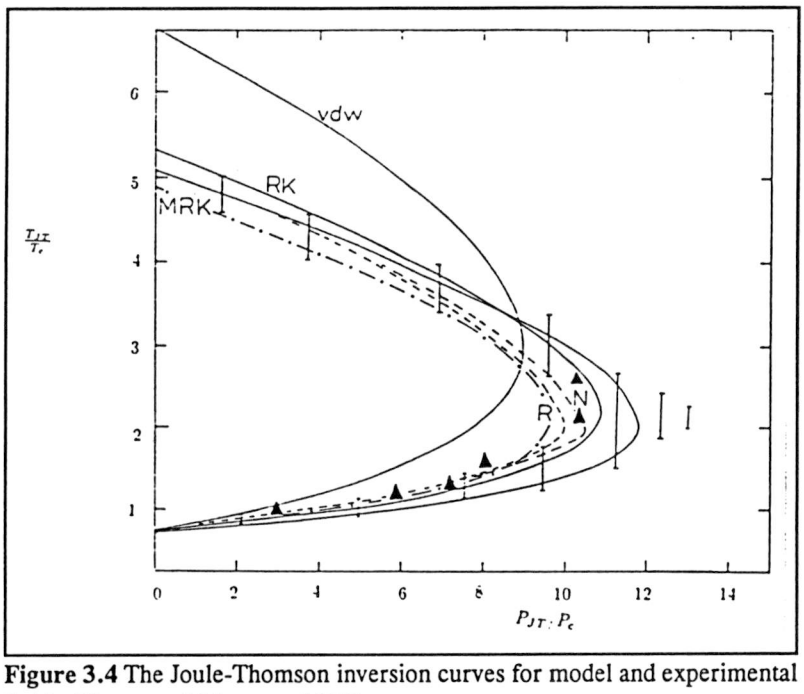

Figure 3.4 The Joule-Thomson inversion curves for model and experimental fluids (Heyes and Llaguno, 1992)

The reduced inversion curves calculated for simple fluids from these equations of state are shown in figure 3.3 along with the Gunn-Chueh-Prausnitz correlation for comparison. Since calculations are made over a large range of temperatures and pressures, it is expected that two-constant equations may have a difficulty in adequately predicting the inversion curve. As can be seen from figure 3.3, this is true for all two-parameter equations of state, except for the RK equation. For the entire range of reduced temperatures and pressures the Dieterici equation is not capable in predicting the inversion curve for simple fluids. The Van der Waals equation also gives poor predictions for the entire range. The Berthelot equation is only in good agreement up to a reduced temperature of 1.3, but fails beyond that. The RK equation however is able to give a good prediction for the entire range. Deviations only occur for the peak, where reduced pressures are slightly too low, and at high temperatures.
Heyes and Llaguno (1992) also considered a modification of the RK equation of state, which they called the **Modified Redlich-Kwong** (MRK) equation,

$$P = \frac{RT}{V-b} - \frac{a}{T^p V(V+qb)} \qquad \textbf{(3.12)}$$

An optimum choice of the parameters q and p was determined by Llaguno and Sanchez (1989) by fitting the reduced form of equation 3.12 with compressibility versus reduced pressure plots. Values of ⅔ for both p and q were obtained. For the original RK equation these values are p=0.5 and q=1. It was found that the MRK equation (dot-dashed line figure 3.4) of state is a better fit to the Gunn-Chueh-Prausnitz correlation than original RK equation (solid line). The maximum reduced pressure calculated by MRK is in better agreement with the Gunn-Chueh-Prausnitz correlation (table 3.1) and the MRK equation is also able to predict the maximum inversion temperature more accurately.

Three-parameter equations of state

In three-parameter equations an extra parameter is added in which the acentric factor is taken into account. Dilay and Heidemann (1986) compared several equations of state, among them the SRK and the PR equations.

Soave-Redlich-Kwong: $$P = \frac{RT}{V-b} - \frac{a(T)}{V(V-b)} \qquad \textbf{(3.13)}$$

Peng-Robinson: $$P = \frac{RT}{V-b} - \frac{a(T)}{V(V+b)+b(V-b)} \qquad \textbf{(3.14)}$$

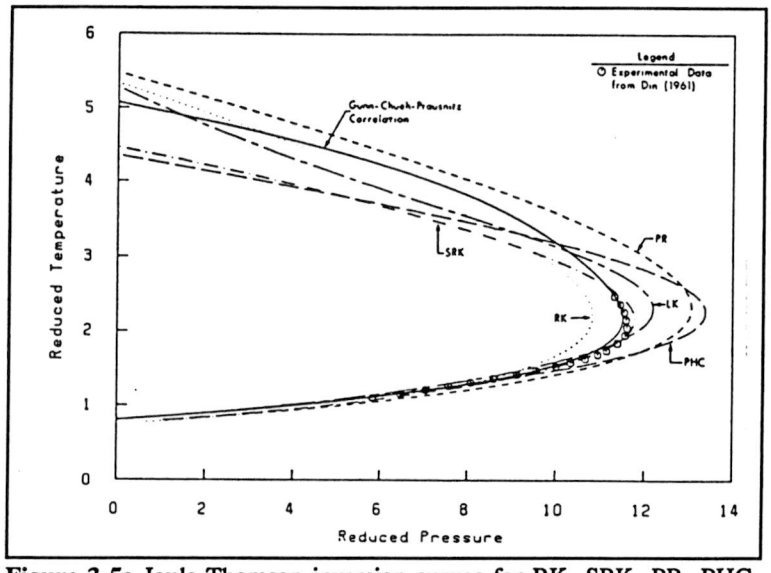

Figure 3.5a Joule-Thomson inversion curves for RK, SRK, PR, PHC, and LK equations of state for ω=0 (Dilay and Heidemann, 1986)

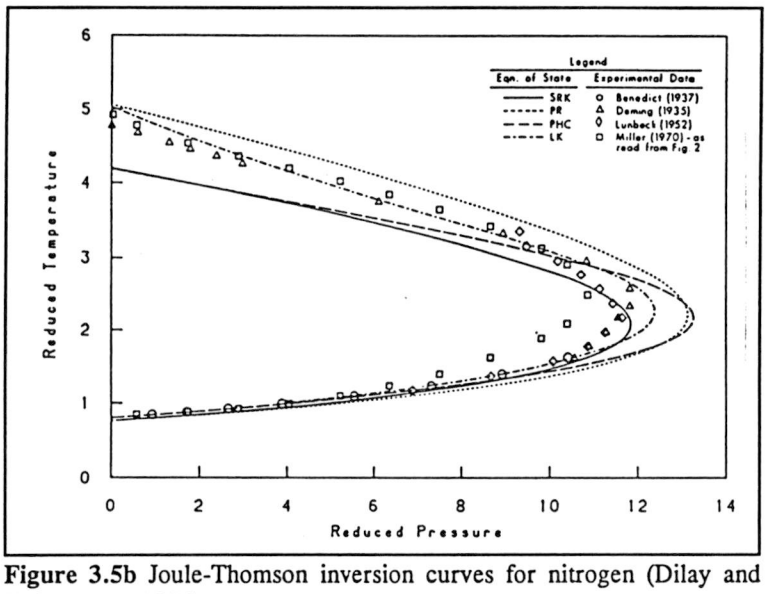

Figure 3.5b Joule-Thomson inversion curves for nitrogen (Dilay and Heidemann, 1986)

In these two equations, the a-parameter is a function of temperature and acentric factor (see appendix B). Figures 3.5a and b show the calculated results for these equations for methane and nitrogen, which are considered as simple fluids ($\omega \approx 0$). The curves are compared with the Gunn-Chueh-Prausnitz correlation, the inversion curve given by the RK equation and with experimental data. The low-temperature part of the curve is well described by all three equations. The peak is closely fitted by SRK but at high reduced temperatures deviations for SRK are larger than for PR and RK. For the upper part of the curve the RK equation gives the best overall results. Rather surprisingly SRK and PR give quite different results for the upper part, despite the similarities between both equations.
To show the influence of the acentric factor on the inversion curve, curves have also been calculated for acentric factors ranging from $\omega=0$ to $\omega=0.25$. In figure 3.6a the result is shown for the Peng-Robinson equation. The figure shows that the acentric factor has only a small effect for the low-temperature part of the curve, but the peak and high-temperature part shows wide variations with the acentric factor.

Other equations of state

In the **Lee-Kesler** (LK) equation the compressibility factor of a fluid is expressed in terms of the compressibility factor of a simple fluid $Z^{(0)}$ and the compressibility factor of a reference fluid $Z^{(r)}$, according to the equation:

$$Z = Z^{(0)} + \frac{\omega}{\omega^{(r)}} [Z^{(r)} - Z^{(0)}] \qquad \textbf{(3.15)}$$

Figures 3.5a and b show that, of all equations tested by Dilay and Heidemann (1986), the LK equation gives the best overall prediction of the Gunn-Chueh-Prausnitz correlation for simple fluids ($\omega=0$). The high temperature branch is best described by the LK the equation and the equation also shows good agreement in the area of the peak. Varying the acentric factor (figure 3.6b), once more shows that the high temperature branch and the peak are sensitive to the acentric factor.

Geană and Feroiu (1992) used a four parameter **general cubic equation of state** to predict the Joule-Thomson inversion curve:

$$P = \frac{RT}{V-b} - \frac{a(T)}{(V-d)^2 + c} \qquad \textbf{(3.16)}$$

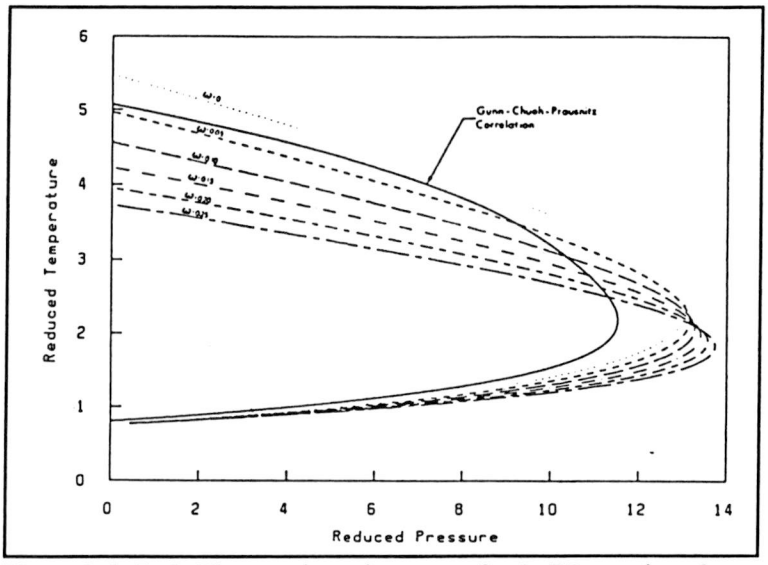

Figure 3.6a Joule-Thomson inversion curves for the PR equation of state (Dilay and Heidemann, 1986)

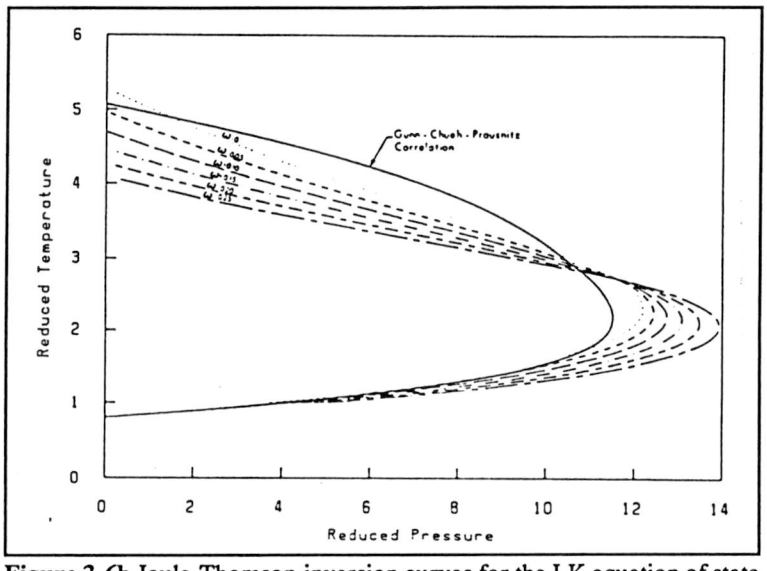

Figure 3.6b Joule-Thomson inversion curves for the LK equation of state (Dilay and Heidemann, 1986)

In this work two functions of reduced temperature were used (appendix B):

$$\beta_1(T_r) = T_r^{-m} \tag{3.17}$$

$$\beta_2(T_r) = \exp[m(1 - T_r)] \tag{3.18}$$

Reduced inversion curves for both functions where calculated for Ar and CO_2 and compared with the Gunn-Chueh-Prausnitz correlation for simple fluids. Figure 3.7a shows that, by using $\beta_1(T_r)$, the calculated inversion curve for argon only corresponds to the Gunn-Chueh-Prausnitz correlation up to a reduced temperature of 1.5. By using the $\beta_2(T_r)$ function the calculated curve is in much better agreement with the correlation. Only the last part of the calculated curve deviates from the experimental one. For comparison the inversion curves calculated by the RK, SRK, PR equations of state are shown in figure 3.7b. In figure 3.8a and b the calculated results are shown for CO_2. For the SRK and the PR equations, acentric factors of ω=0 for Ar and of ω=0.225 for CO_2 were used. Both figures show that the best results are obtained with the GEoS using the $\beta_2(T_r)$ function.

3.1.4 Direct molecular simulation

Heyes and Llaguno (1992) proposed a new equilibrium molecular dynamics procedure for determining directly the Joule-Thomson inversion curve from model simulation fluids. This method has the advantage that the inversion curve does not need to come from a predetermined equation of state. The simulation method was tested for the **Lennard-Jones** (LJ) fluid and compared with the **Van der Waals**, the **Redlich-Kwong** (RK) and the **modified Redlich-Kwong** (MRK) equations of state. Because direct calculations are somewhat cumbersome, reference is made to the original work for the exact simulation method. Figure 3.4 shows the results calculated by Heyes and Llaguno (filled triangles) and the curve prediction by the equations of state (solid lines). Heyes and Llaguno concluded that the simulation route to the inversion temperature works well along the lower branch of the curve but gives steadily poorer results along the upper branch. Heyes and Llaguno therefore recommended to use an equation of state for the upper branch. For the lower branch the direct route is at least as accurate.

3.2 Inversion curves for gas-mixtures

In the previous paragraph inversion curves were calculated only for pure components. When dealing with gas-mixtures it is also important to know how the inversion curve is affected by composition.

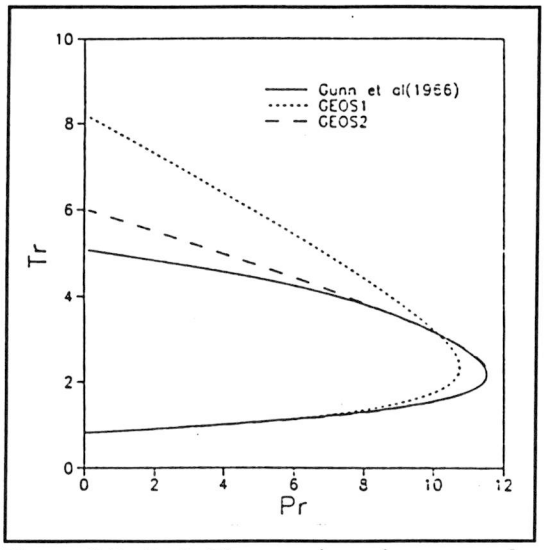

Figure 3.7a Joule-Thomson inversion curves for Ar by GEoS with functions $\beta_1(T_r)$ and $\beta_2(T_r)$ (Geană and Feroiu, 1992)

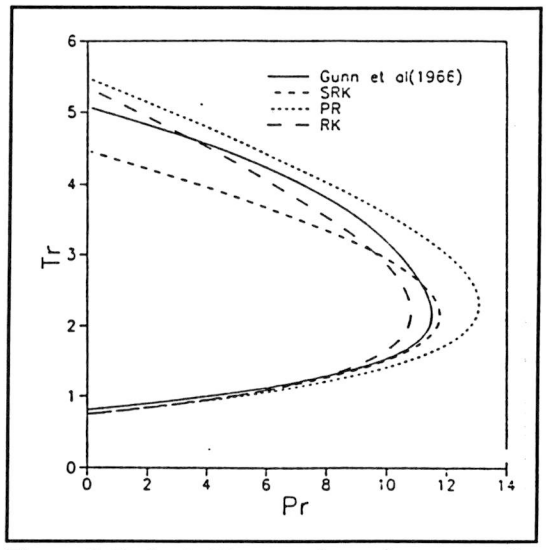

Figure 3.7b Joule-Thomson inversion curves for Ar calculated by SRK, PR and RK equations of state (Geană and Feroiu, 1992)

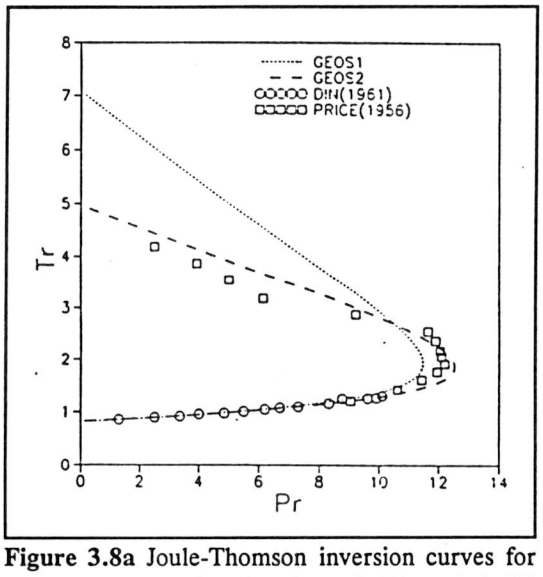

Figure 3.8a Joule-Thomson inversion curves for CO_2 by GEoS with functions $\beta_1(T_r)$ and $\beta_2(T_r)$ (Geană and Feroiu, 1992)

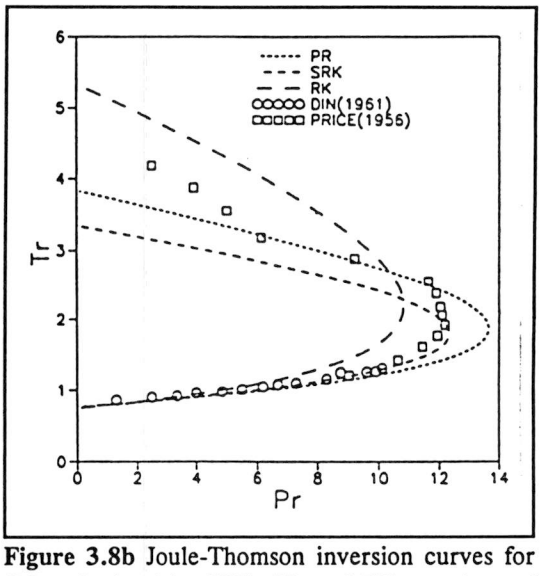

Figure 3.8b Joule-Thomson inversion curves for CO_2 calculated by SRK, PR and RK equations of state (Geană and Feroiu, 1992)

To calculate the inversion curve for gas mixtures Gunn et al. (1966) proposed the following method. In order to apply the Gunn-Chueh-Prausnitz correlation for gas-mixtures it is necessary to express the reducing constants as a function of composition. Gunn et al. recommended to calculate the pseudo-critical reducing parameters as follows:

$$T_{cm} = \sum_{i}^{N} y_i T_{ci} \tag{3.19}$$

$$V_{cm} = \sum_{i}^{N} y_i V_{ci} \tag{3.20}$$

$$P_{cm} = \frac{R T_{cm}}{V_{cm}} \sum_{i}^{N} y_i Z_{ci} \tag{3.21}$$

where Z_{ci} is the critical compressibility factor of component i:

$$Z_{ci} = 0.291 - 0.08\,\omega_i \tag{3.22}$$

These equations may be used for small molecules, i.e. for mixtures where

$$\sum_{i}^{N} y_i\,\omega_i < 0.1 \tag{3.23}$$

The inversion pressure for a mixture can now be estimated:

$$\frac{P}{P_{cm}} = f_0\left(\frac{T}{T_{cm}}\right) + \alpha_m f_{He}\left(\frac{T}{T_{cm}}\right) \tag{3.24}$$

where $f_0(T/T_{cm})$ is obtained from equation 3.2, α_m is de Broglie wavelength ratio calculated from a mole fraction average of the individual de Broglie wavelengths

$$\alpha_m = 37.63\left[\sum_{i}^{N} \frac{y_i}{\sqrt{(m_i T_{ci})}}\right] \tag{3.25}$$

and $f_{He}(T/T_{cm})$ is calculated from the quantum deviation function for helium-4 derived by Gunn et al.:

$$f_{He}(T_r) = 34.428 - 64.471\,T_r + 44.780\,T_r^2 - 14.344\,T_r^3 + 2.2071\,T_r^4 - 0.12909\,T_r^5 \tag{3.26}$$

Figure 3.9 shows the results for a methane-hydrogen mixture at fixed temperature. This figure shows that the experimental and calculated values of inversion pressures deviate strongly from a linear mole-fraction average of the inversion pressure and that a maximum pressure occurs.

The occurrence of a maximum inversion pressure appears to be common for those binary mixtures whose pure-component reduced temperatures lie on different sides of the maximum of the generalized inversion curve shown in figure 3.1. In table 3.2 another example of the influence of composition is given for a methane-butane mixture.
These two examples show two important things: first of all that the locus of the inversion is not only determined by pressure and temperature but also by composition and that inversion pressures at fixed temperatures can deviate strongly from a linear average of pure-component inversion pressures. When dealing with gas-condensates (which are multi-component mixtures), this must be taken into account.

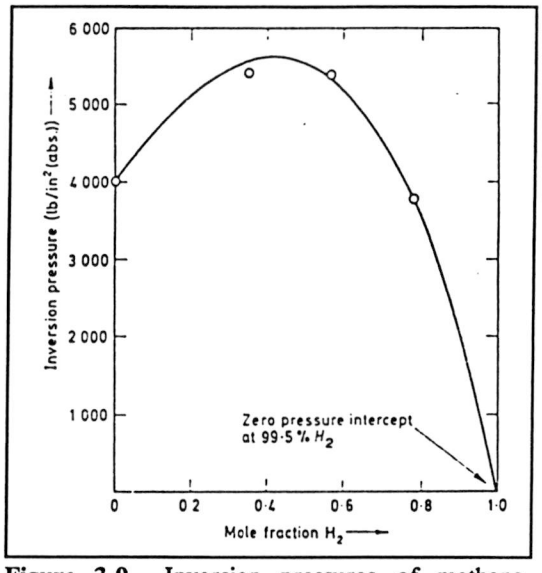

Figure 3.9 Inversion pressures of methane-hydrogen mixtures at 214 K (Gunn et al.,1966)

Table 3.2 Inversion pressures (lb/in²(abs.)) for methane-butane mixtures

Inversion temp.(°F)	Mixture containing 79.97 mole% methane			Mixture containing 60.02 mole% methane		
	Exp.	Calc.	%Dev.	Exp.	Calc.	%Dev.
130	5645	5551	-1.7	4000	3822	-4.5
190	6394	6196	-3.1	4891	4673	-4.5
250	6931	6652	-4.0	5718	5346	-6.5
310	7261	6955	-4.2	6275	5865	-6.5
370	7525	7136	-5.2	6593	6241	-5.3
430	7568	7222	-4.6	7132	6538	-8.3

4. Prediction of the Temperature Effect

When calculating the temperature changes occurring on Joule-Thomson expansion of fluids, a few things have to be considered. First of all, a method has to be chosen to calculate the temperature change. Secondly, one must be aware of the possibility of phase-transitions to occur and finally, the influence of composition in multi-component systems one temperature change must also be considered.

4.1 Methods to calculate temperature changes

To calculate the temperature effect due to the Joule-Thomson expansion of a gas, two methods can be adopted: an iteration method which calculates the temperature changes using the averaged Joule-Thomson coefficient μ_{JT} and a iteration method, in which the final temperature is found by equalizing the value of enthalpy before and after expansion.

Chou et al. (1992) predicted the final temperature following expansion of nitrogen gas by using the averaged Joule-Thomson coefficient. Based on the conclusions of Hirose et al. (1990), they used the RK equation of state to calculate Joule-Thomson coefficients. To determine the value of the specific volume V, they used the Benedict-Webb-Rubin (BWR) equation, due to its higher accuracy. Two sets different sets of BWR constants were used in their work. In order to predict the final temperature one needs to know not only the values of the Joule-Thomson coefficient before and after expansion, but also how to simulate the highly non-linear process of expansion. An iteration process was used given by Wark (1989), which involves the average μ_{JT} in the given pressure range and the iteratively-corrected final temperature. In the simulation the pressure jump is divided into k steps. Chou et al. showed that a minimum number of five steps is required and that for a larger number of steps differences between the results are rather small. Figure 4.1 shows calculated temperatures after expansion T_a for variable starting temperatures T_b. Chou et al. concluded that the deviations shown in figure 4.1 are due to incorrect lower values of μ_{JT}, which are mainly caused by unsuitable modelling of $T(\partial V/\partial T)_P$ and V in equation 2.7.

Chou et al. also calculated the final temperature after expansion of nitrogen using the departure function for enthalpy. The departure function is defined as $H-H^0$, where H^0 is the value of H at the same temperature but in an ideal gas state and at a reference pressure (P=0). The following equations were used:

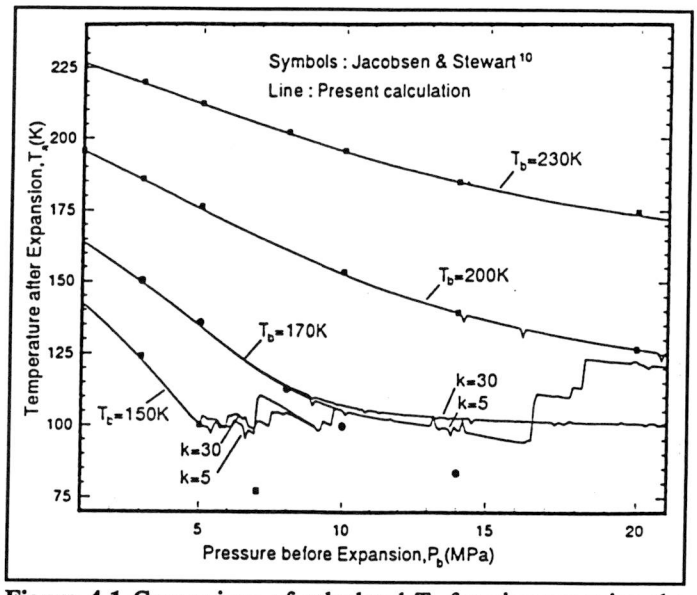

Figure 4.1 Comparison of calculated T_a for nitrogen using the BWR equation (Chou et al., 1992)

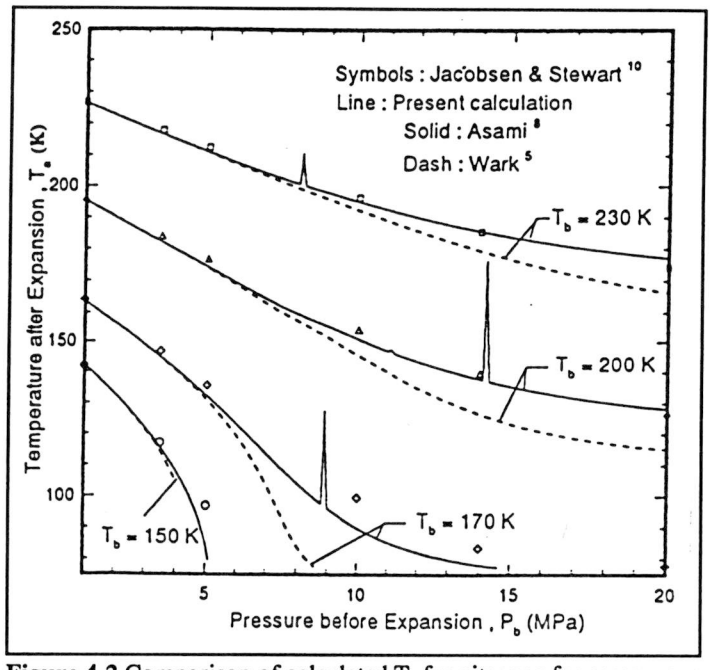

Figure 4.2 Comparison of calculated T_a for nitrogen for cases were T_b is 230, 200, 170 and 150 K (Chou et al., 1992)

$$H - H^0 = (A - A^0) + T(S - S^0) + RT(Z - 1) \tag{4.1}$$

$$A - A^0 = -\int_{\infty}^{V} [P - (RT/V)]dV - RT\ln(V/V^0) \tag{4.2}$$

$$S - S^0 = -[\partial(A - A^0)/\partial T]_V \tag{4.3}$$

$$H^0 = H_{ref} + \int_{T_0}^{T} C_{P_0} dT \tag{4.4}$$

Chou et al. used the RK equation to calculate H-H^0 and again used the BWR equation to calculate the specific volume V. Results are shown in figure 4.2 for varying temperatures before expansion T_b. For lower temperatures figure 4.2 shows deviations for the temperature after expansion T_a at higher pressures. By comparing calculated enthalpies to experimental data, Chou et al. concluded that these deviations in T_a are caused by the incorrect lower values of calculated H.

4.2 Phase-transitions during expansion

When single or multi-component systems stay in a single phase during pressure relief, the temperature change can be solved by iterative solution of the enthalpy balance equation. However when condensation takes place during expansion, the Joule-Thomson effect has to calculated in the two phase region. In the work by Nagy (1991) the computation of natural gas Joule-Thomson effect in single or vapour-liquid systems is considered.
The main difference between computation of the Joule-Thomson effect in the single and two phase region consists in:

- calculation of vapour and liquid compositions during throttling
- necessity of computation residual functions for both phases
- necessity of computation of phase fraction in system

For condensation to occur the final temperature must be lower than the dew temperature (figure 4.3). The main problem encountered for the two phase Joule-Thomson effect is to verify if two phases exist at pressure P_2. Nagy (1991) solved this by applying the Gibbs tangent plane criterion, described by Michelsen (1982), to test the thermodynamic stability of

the initial and final phases. If a phase is instable, the problem is solve using a isenthalpic flash procedure. Besides the material balances for all component, the following equilibrium condition equations are required:

$$\hat{f}_i^v = \hat{f}_i^l \qquad \{i = 1, \ldots, N\} \tag{4.5}$$

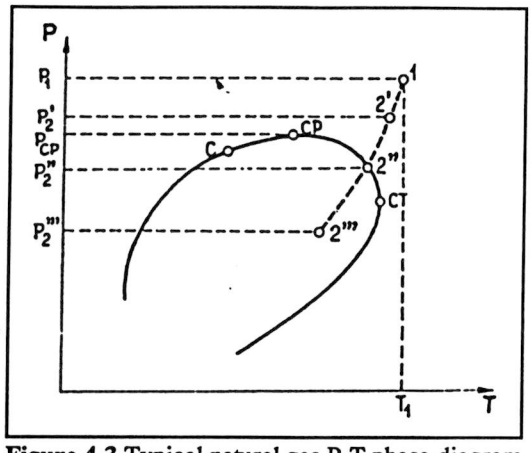

Figure 4.3 Typical natural gas P-T phase diagram (Nagy, 1991)

4.3 Influence of fluid composition on temperature effect

In §3.2 is was shown that the composition of gas-mixtures can have a significant effect on the locus of the inversion curve. Therefore, the composition will also effect the temperature change due to expansion. The influence of composition is complex because it depends not only on number and kind of components, but also on variations of composition and thus possibilities are unlimited. Still, to give an impression of the composition influence, an example is given by the temperature curves calculated by Laurence (1984) in appendix C. The curves were calculated for natural gases of different compositions by using the SRK equation of state. These results show that for natural gas systems, with steadily increasing fractions of heavier components, the temperature change in the same pressure range can change from cooling to heating.

5. Gas-Condensate Reservoirs

5.1 Characterization of gas-condensates

In the previous chapters it was shown that the temperature effect due to Joule-Thomson expansion is not only by influenced initial pressure and temperature but, when dealing with gas-mixtures, also by composition. Therefore, in order to predict the Joule-Thomson inversion effect that might occur at expansion of gas-condensates, it is first necessary to characterize these gas-condensate systems.

5.1.1 Composition ranges for gas-condensate systems

Gas-condensate systems, like all petroleum reservoir fluids, are multi-component mixtures consisting primarily of hydrocarbons which are separated into three classes:

- Paraffins (or alkanes)
- Naphthenes (or cycloalkanes)
- Aromatics

In addition to the hydrocarbons, also nitrogen, carbon dioxide, and hydrogen sulphide are often found in petroleum mixtures. Finally, petroleum mixtures may contain helium, mercury and metal-organic compounds. Table 5.1 shows typical compositions of petroleum reservoir fluids. Compared with natural gas the methane content of gas-condensates is lower and the fraction heavier ends (C_{2+}) is larger. Compared with crude oils table 5.1 shows that gas-condensates contain much lower C_{7+} fractions.

The compositions of gas-condensate systems can vary widely and will therefore, as mentioned earlier, have a significant effect on the locus of the inversion curve and the temperature change due to expansion. To give a general idea how wide these variations are, compositions of several gas-condensates taken from Pedersen and Thomassen (1988) and Montel (1994) are shown in table D.1 in appendix D.
If we wish to predict the Joule-Thomson effect for high pressure high temperature gas-condensate reservoirs as mentioned in the introduction, it is necessary to have reliable composition data. Data for such high pressure high temperature systems are very scarce. Montel (1994) provided data sets for two gas-condensate mixtures, but besides these

compositions, none were available in open literature. The other gas-condensates for which composition data are found, have much lower reservoir pressures, typically in the range of 300 to 600 bar.

Table 5.1 Typical molar compositions of petroleum reservoir fluids†

Component	Gas	Gas-condensate	Volatile Oil	Black Oil
N_2	0.3	0.71	1.67	0.67
CO_2	1.1	8.65	2.18	2.11
C_1	90.0	70.86	60.51	34.93
C_2	4.9	8.53	7.52	7.00
C_3	1.9	4.95	4.74	7.82
C_4 (i+n)	1.1	2.00	4.12	5.48
C_5 (i+n)	0.4	0.81	2.97	3.80
C_6 (i+n)	6^+: 0.3	0.46	1.99	3.04
C_7		0.61	2.45	4.39
C_8		0.71	2.41	4.71
C_9		0.39	1.69	3.21
C_{10}		0.28	1.42	1.79
C_{11}		0.20	1.02	1.72
C_{12}		0.15	12^+: 5.31	1.74
C_{13}		0.11		1.74
C_{14}		0.10		1.35
C_{15}		0.07		1.34
C_{16}		0.05		1.06
C_{17}		17^+: 0.37		1.02
C_{18}				1.00
C_{19}				0.9
C_{20}				20^+: 9.18

† Pedersen et al. (1989)

5.1.2 Pressure and temperature ranges

Bradley (1989) states that gas-condensate reservoirs may occur at pressures below 2,000 psia (138 bar) and temperatures below 100 °F (38 °C) and probably can occur at any higher fluid pressures and temperatures within reach of drill. Most known gas-condensate reservoirs are in the range of 3,000 to 8,000 psia (207 to 552 bar) and 200 to 400 °F (93 to 204 °C).
In the introduction gas-condensate reservoir conditions of approximately 1,000 bar and 100

to 200 °C were mentioned which lie well outside this pressure range. However in the open literature, publications describing these kind of high pressure high temperature (HPHT) reservoirs are hardly found. For gas-condensates only one such reservoir has been found, reported by Baker and Price (1990). Typical reservoir conditions are in the range of 16,000 psia (1,100 bar) and 400 °F (200 °C). However, due to confidentiality requirements the actual composition of this light gas-condensate has not been published. The two samples of gas-condensates provided by Montel (1994), were taken at reservoir conditions of 1100 bar and 185-195 °C.

5.1.3 Phase behaviour of gas-condensates

When describing the phase behaviour of multi-component mixtures, such as gas-condensate systems, phase-diagrams as shown in figure 5.1 are used (this is the predicted phase envelope of the HPHT reservoir described by Baker and Price, 1990).
The figure gives the region for which the mixture forms two phases. In these multicomponent systems, the critical temperature is no longer the maximum temperature at which two phases can exist. Instead the phase envelope is bounded by a *cricondentherm*, the maximum temperature for formation of two phases, and a *cricondenbar*. For a gas-condensate systems typical reservoir conditions lie outside the phase envelope and thus the gas is a single phase.
A phase-diagram corresponds with a fixed composition. This is emphasized by figures 5.2a-c which show that the phase-diagram is strongly affected by variations in composition of gas-condensate systems (table 5.2).
Describing the phase behaviour of a gas-condensate is generally very difficult, because phase behaviour of a gas-condensate is very much dependent on the heaviest constituents of the mixture. For example, a dew point pressure is highly sensitive to the molecular weights of the heaviest components and also a cubic equation of state is expected to be less accurate when dealing with larger molecules. While the lighter constituents of reservoir fluids are well-defined individual components, the heavier (C_7^+) fractions however are mixtures of different components. In order to simulate the phase behaviour of a gas-condensate it is therefore necessary that the C_7^+ fraction is characterized.

5.1.4 Characterization of the heavy fractions

To use equations of state like the Soave-Redlich-Kwong or the Peng-Robinson equations for petroleum mixtures, the critical temperature T_c, critical pressure P_c and the acentric factor ω, are needed for each component.

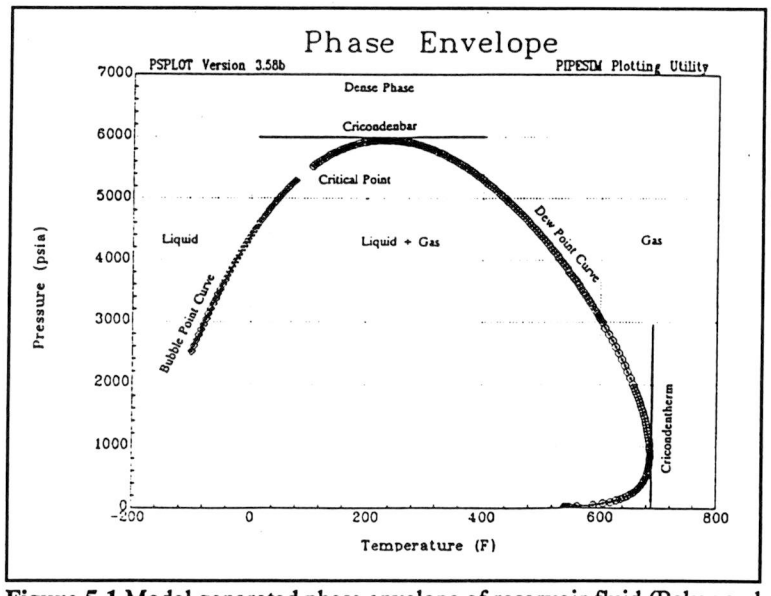

Figure 5.1 Model generated phase envelope of reservoir fluid (Baker and Price, 1990)

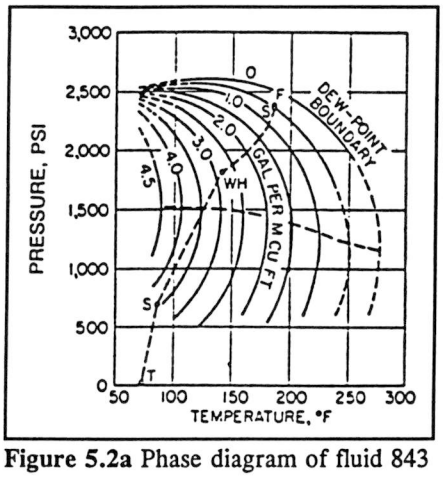

Figure 5.2a Phase diagram of fluid 843

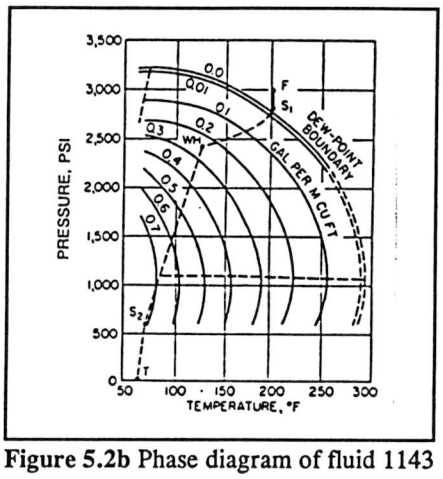

Figure 5.2b Phase diagram of fluid 1143

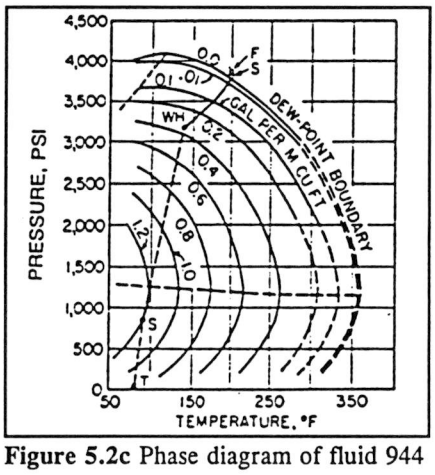

Figure 5.2c Phase diagram of fluid 944

Table 5.3 Hydrocarbon analyses of example gas-condensates †

Component	Condensate 843	Condensate 944	Condensate 1143
N_2	0.01375	0.00075	0.01480
CO_2	0.00794	0.00130	0.00695
C_1	0.76432	0.89498	0.89045
C_2	0.07923	0.04555	0.04691
C_3	0.04301	0.01909	0.01393
C_4	0.03060	0.00958	0.00795
C_5	0.01718	0.00475	0.00424
C_6	0.01405	0.00385	0.00379
C_7^+	0.02992	0.02015	0.01098

† Bradley (1989)

Because the heavy fractions are normally split in boiling point fractions, each consisting of many different components, these parameters are, un-like the lighter constituents, are not available. Instead, the critical properties and the acentric factor are estimated from measurable properties using empirical correlations. A number of characterization procedures have been published

1. Lee-Kesler Correlations (Kesler and Lee, 1976)

$$T_c = 341.7 + 811\,SG + (0.4244 + 0.1174\,SG)\,T_B + (0.4669 - 3.2623\,SG)\,10^{-5}/T_B \tag{4.1}$$

$$\ln P_c = 8.3634 - 0.0566/SG - (0.24244 + 2.2898/SG + 0.11857/SG^2)\,10^{-3} + (1.4685 + 3.648/SG + 0.47227/SG^2)\,10^{-7}\,T_B^2 - (0.42019 + 1.6977/SG^2)\,10^{-10}\,T_B^3 \tag{4.2}$$

$$\omega = \frac{\ln P_{Br} - 5.92714 + 6.09648\,T_{Br}^{-1} + 1.28862 \ln T_{Br} - 0.169347\,T_{Br}^6}{15.2518 - 15.6875\,T_{Br} - 134721 \ln T_{Br} + 0.43577\,T_{Tr}^6} \tag{4.3}$$

(for $T_{Br} < 0.8$*)*

$$\omega = -7.904 + 0.1352K - 0.007465K^2 + 8.359\,T_{Br} + (1.408 - 0.001063K)\,T_{Br}^{-1} \tag{4.4}$$

(for $T_{Br} > 0.8$*)*

The boiling point T_B and T_c are in Rankin, the specific gravity SG in 60 °F/60 °F, and P_c in

psia. T_{Br} equals T_B/T_c and P_{Br} equals P_B/P_c, where P_B is the pressure at T_B and K is the Watson characterization factor which equals $T_B^{1/3}/SG$.

2. Winn Relations (Winn, 1957; Sim and Daubert, 1980)

$$T_c = \frac{\exp\left[4.2009\, T_B^{0.08615}\, SG^{0.04614}\right]}{1.8} \tag{4.5}$$

$$P_c = 6.1483\, 10^{12}\, T_B^{-2.3177}\, SG^{2.4853} \tag{4.6}$$

$$MW = 5.805\, 10^{-5} \left[\frac{T_B^{2.3776}}{SG^{0.9371}}\right] \tag{4.7}$$

where T_B and T_c are in K, SG in 15 °C/15 °C, and P_c in Pa.

3. Cavett (1964) Relations

$$\begin{aligned} T_c = {} & 768.071 + 1.7134\, T_B - 0.10834\, 10^{2}\, T_B^2 + 0.3889\, 10^{6}\, T_B^3 \\ & - 0.89213\, 10^{-2}\, T_B API + 0.53095\, 10^{-6}\, T_B^2 API + 0.32712\, 10^{-7}\, T_B^2 API^2 \end{aligned} \tag{4.8}$$

$$\begin{aligned} \log P_c = {} & 2.829 + 0.9412\, 10^{-3}\, T_B - 0.30475\, 10^{-5}\, T_B^2 + 0.15141\, 10^{-8}\, T_B^3 - 0.20876\, 10^{-4}\, T_B API \\ & + 0.11048\, 10^{-7}\, T_B^2 API + 0.1395\, 10^{-9}\, T_B^2 API^2 - 0.4827\, 10^{-7}\, T_B API^2 \end{aligned} \tag{4.9}$$

In these equations, API = 141.5/SG - 131.5, where SG is the 60 °F/60 °F specific gravity. The critical temperature T_c and the boiling point of the fraction, T_B, are given in °F, and the critical pressure P_c in psia. T_{Br} is the reduced boiling point (T_B/T_c) and P_{Br} the reduced pressure (P_B/P_c).

4. Edminster's (1958) Acentric Factor

$$\omega = \frac{3}{7}\left[\frac{\log P_c}{T_c/T_B - 1}\right] - 1 \tag{4.10}$$

where P_c is in atmospheres.

5. The correlations of Riazi and Duabert (1980)

$$T_c = 24.2787\, T_B^{0.58848}\, SG^{0.3596} \tag{4.11}$$

$$P_c = 3.12281\, 10^9\, T_B^{-2.3125}\, SG^{2.3201} \tag{4.12}$$

where T_c and T_B are in Rankin, SG in 60 °F/60 °F, and P_c in psia.

6. Relations of Pedersen et al. (1988)

Often, data on T_B is not available and T_B is therefore estimated from the available physical data, MW and ρ. This is in fact an unnecessary intermediated step and therefore Pedersen et al. (1988) suggested to use correlations, which directly correlate T_c, P_c and ω with MW and ρ using the following expressions:

$$T_c = c_1 \rho + c_2 \ln MW + c_3 MW + c_4 MW^{-1} \tag{7.13}$$

$$\ln P_c = d_1 + d_2 \rho + d_3 MW^{-1} + d_4 MW^{-2} \tag{7.14}$$

$$m = e_1 + e_2 MW + e_3 \rho + e_4 MW^2 \tag{7.15}$$

where m is a function of the acentric factor (see appendix B), from which ω can be calculated. Table 7.2 contains optimum values for the parameters c_1-c_4, d_1-d_4, e_1-e_4 for use with the SRK equation.

7. Relations of Aasberg-Petersen and Stenby (1991)

Aasberg-Petersen and Stenby (1991) used equations to calculated T_c and P_c, which have the same functional form as those from Pedersen and Thomassen (1988). However, ρ is replaced by SG. The value of the parameters are slightly different (table 7.2). The value of omega is calculated directly from:

$$\omega = e_1 + e_2 MW + e_3 SG + e_4 MW^2 \tag{7.16}$$

5.2 Joule-Thomson inversion effect at expansion of gas-condensates

Now gas-condensates have been characterized, the Joule- Thomson expansion of these systems can be considered. As mentioned earlier, heating of these gas-condensates, due to the inversion effect, will take place for systems at high temperatures and even more important at high pressures. Unfortunately for such systems very little is reported on Joule-Thomson effects. Two practical examples were found and one theoretical example in which calculations have been made.

Table 7.2 Optimum values of the coefficients in eqns. 7.13-7.16

	Pedersen (1988)	Aasberg-Petersen (1991)
c_1	$1.6312\ 10^{2}$	190.8 ± 37
c_2	$8.6052\ 10^{0}$	87.70 ± 3.1
c_3	$4.3475\ 10^{-1}$	0.6387 ± 0.087
c_4	$-1.8774\ 10^{3}$	-5247.7 ± 2830
d_1	$-1.3408\ 10^{-1}$	-0.5836 ± 0.097
d_2	2.5019	2.3211 ± 0.23
d_3	$2.0846\ 10^{2}$	282.2 ± 24
d_4	$-3.9872\ 10^{3}$	-4484.9 ± 2100
e_1	$7.4310\ 10^{-1}$	$2.829\ 10^{-2} \pm 6.4\ 10^{-2}$
e_2	$4.8122\ 10^{-3}$	$4.248\ 10^{-4} \pm 4.7\ 10^{-4}$
e_3	$9.6707\ 10^{-3}$	$1.156\ 10^{-2} \pm 3.0\ 10^{-3}$
e_4	$-3.7184\ 10^{-6}$	$-4.069\ 10^{-6} \pm 7.5\ 10^{-7}$

Baker and Price (1990) reported a high-pressure high-temperature (HPHT) well, where reservoir conditions are in the range of 16,000 psia and 400 °F. During a series of production tests it was observed that downhole temperatures were significantly in excess of the undisturbed reservoir temperature. In one particular test, a bottom hole temperature rise of some 15 °F was observed when reservoir drawdown was approximately 7,000 psia. These temperature rises seemed to be in conflict with expected behaviour of the gas because one would expect a Joule-Thomson cooling at expansion. The temperature of the HPHT well was within the region where cooling can occur (figure 5.3), but because the reservoir pressure was well above the maximum inversion pressure it is not possible to observe cooling until pressure decreases to approximately 8,000 psia.

Jones (1988) also reported that, due to the Joule-Thomson inversion effect, bottomhole temperature increased while flowing. As a result the wellbore was heated to above the normal static reservoir temperature during production. The magnitude of this temperature change depends not only, as earlier mentioned, on the fluid composition, pressure and temperature, but also on drawdown. Unfortunately, nothing is mentioned about reservoir conditions or composition of the reservoir fluid.

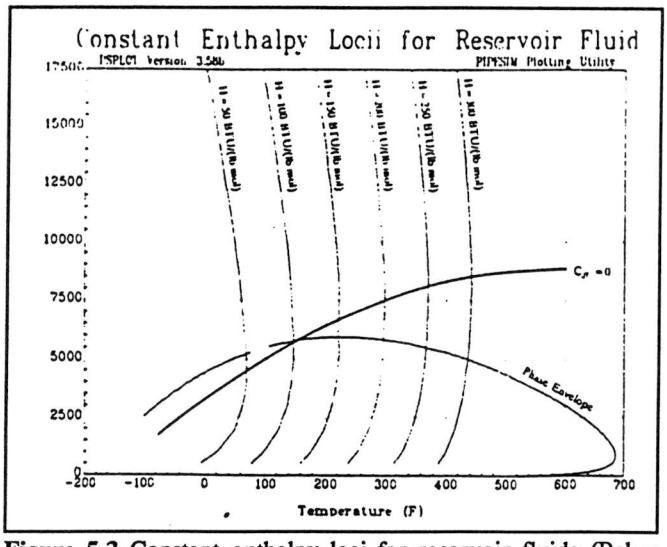

Figure 5.3 Constant enthalpy loci for reservoir fluids (Baker and Price, 1990)

The temperature curves calculated by Laurence (1984) can be used as a theoretical example of the heating of gas-condensates. These curves were calculate using the SRK equation of state. Although referred to as natural gases by Laurence, the compositions with a molecular weight higher than approximately 25 (see appendix C) can be considered as gas-condensates. These results show that a temperature rise will occur when expansion takes place from high pressure (10.000 psia) to a lower pressure (for example 5.000 psia). More important is that they show that the temperature rise increases with increasing fraction of heavy components.

6. Discussion and Conclusions

In this review it has been shown that a fluid can heat at expansion due to the Joule-Thomson inversion effect. When a fluid is above its maximum inversion temperature heating will always take place at expansion. Beneath this maximum temperature the fluid will heat when the initial conditions of this fluid lie outside the inversion curve. This heating will continue to take place until the inversion curve is crossed.
It was also shown that the temperature change, due to expansion, is not only a function of initial pressure and temperature but also of fluid composition and when dealing with flowing fluids of drawdown. When calculating temperature changes one must also be aware of the possibility that phase-transitions take place.
The examples in §5.2 show that for gas-condensates systems at high pressure and high temperature, heating can take place at expansion due to the Joule-Thomson inversion effect. When predicting this temperature rise the following must be considered:

1) accurately characterizing the gas-condensate system
2) choosing an appropriate equation of state

ad 1) Besides the reservoir pressure and temperature, it is essential to know the composition of the gas-condensate system, because this will have a great effect on temperature changes. Because no composition data for these high pressure high temperature reservoirs are currently available, accurate estimates will have to be made.

ad 2) An equation of state must be chosen to calculate fluid behaviour, inversion curves, departure functions and derived properties as specific heats. The equation must be able to calculate these properties over a wide range of pressures and temperatures and for a mixture of several (larger) components. Also the fraction of the heavier components must be accurately characterized because of their large influence on calculated results.

List of Symbols

Nomenclature			**Unit**
a,b	:	parameters in equations of state	[-]
C_P	:	specific heat at constant pressure	J mole^{-1} K^{-1}
C_V	:	specific heat at constant volume	J mole^{-1} K^{-1}
f	:	fugacity	Pa
g	:	gravitational constant	m s^{-2}
H	:	enthalpy	J mole^{-1}
MW	:	molecular weight	g mole^{-1}
N	:	number of components	[-]
P	:	pressure	Pa
Q	:	heat	kW
R	:	gas constant	J mole^{-1} K^{-1}
S	:	entropy	J mole^{-1} K^{-1}
SG	:	specific gravity	[-]
T	:	temperature	K
v	:	velocity	m s^{-1}
V	:	molar volume	m^3
W	:	work	kW
x_i	:	mole fraction in liquid phase	[-]
y_i	:	mole fraction in vapour phase	[-]
z	:	height	m
Z	:	compressibility factor	[-]

greek symbols

α_m	:	de Broglie wavelength	[-]
μ_{JT}	:	Joule-Thomson coefficient	K Pa^{-1}
ω	:	acentric factor	[-]

superscripts

id	:	ideal
(0)	:	simple fluid
(r)	:	reference fluid

subscripts

B	:	boiling point
c	:	critical property
r	:	reduced property
m	:	mixed property

References

Aasberg-Petersen, K., Stenby, E., **Prediction of Thermodynamic Properties of Oil and Gas Condensate Mixtures**, *Ind. Eng. Chem. Res.*, **1991**, 30, 248-254.

Alhert, R.C., Wenzel, L.A., *AIChE J.*, **1969**, 15, 256.

Baker, A.C. et al, **Modelling the performance of high-pressure high-temperature wells**, SPE European Petroleum Conference, 21-24 october 1990, 217-230.

Bradley, **Petroleum Engineering Handbook**, SPE, Richardson, TX, USA, 2nd ed. 1989.

Budenholzer, R.A., Sage, B.H., Lacey, W.N, **Joule-Thomson Coefficient of Methane**, *Ind. Eng. Chem.*, Vol.31, No.3, March 1939, 369-374.

Budenholzer, R.A., Sage, B.H., Lacey, W.N, **Joule-Thomson Coefficients for Gaseous Mixtures of Methane and Ethane**, *Ind. Eng. Chem.*, Vol.31, No.10, October 1939, 1288-1292.

Budenholzer, R.A., Sage, B.H., Lacey, W.N, **Joule-Thomson Coefficients in the Methane-Propane System**, *Ind. Eng. Chem.*, Vol.34, No.7, July 1942, 878-882.

Budenholzer, R.A., Sage, B.H., Lacey, W.N, **Joule-Thomson Coefficients for Gaseous Mixtures of Methane and n-Butane**, *Ind. Eng. Chem.*, Vol.32, No.3, March 1940, 384-387.

Cavett, R.H., **Physical Data for Distillation Calculation, Vapor-Liquid Equilibria**, 27th Midyear Meeting, API Division of Refining, San Francisco, CA, May 15, 1964.

Chou, F.C., Wu, S.M., Pai, C.F., **Prediction of final temperature following Joule-Thomson expansion of nitrogen gas**, *Cryogenics*, 1993 Vol.33, No.9, 857-862.

Corner, J., **The Joule-Thomson inversion curves of recent equations of state**, *Trans. Farad. Soc.*, **35**, (1939), 784-791.

Dilay, G.W., Heidemann, R.A, **Calculation of Joule-Thomson Inversion Curves from Equations of State**, *Ind. Eng. Chem. Fundam.*, Vol.25, No.1, 1986, 152-158.

Edminster, W.C., **Applications of Thermodynamics to Hydrocarbon Processing; Part XV Joule-Thomson Effect**, *Petroleum Refiner*, Vol.37, 1958, 173-179.

Edminster, W.C., **Applied Hydrocarbon Thermodynamics. Part 4. Compressibilty Factors and Equations of State** *Petroleum Refiner*, Vol.28, No.1, January 1949, 128-133.

Geană, D., Feroiu, V., **Calculation of Joule-Thomson inversion curves from a general cubic equation of state**, *Fluid Phase Equilibria*, 77 (1992) 121-132.

Gunn, R.D., Chueh, P.L., Prausnitz, J.M., **Inversion temperatures and pressures for cryogenic gases and their mixtures**, *Cryogenics*, Vol.6, No.6, 1966, 324-329.

Heyes, D.M., Llaguno C.T., **Computer simulation and equation of state study of the Boyle and inversion temperature of simple fluids**, *Chemical Physics* 168 (1992) 61-68.

Yasuo Hirose, Tsuyoshi Kitazawa, Toshinobu Yoshida, **The Joule-Thomson coefficient by formula**

manipulation, *Ind. Eng. Chem. Res.* **1990,** 29, 1555-1558.

Johnston, H.L., *J. Am. Chem. Soc.*, **1949,** 108, 23102.

Jones, C., **The use of bottomhole temperature variations in production testings,** SPE European Petroleum Conference, 16-19 october 1988, 423-431.

Juris, K., Wenzel, L.A., **A Study of Inversion Curves,** *AIChE Journal* (Vol.18, No.4) July, 1972, 684-688.

Kesler, M.G., and Lee, B.I., **Improve Prediction of Enthalpy of Fractions,** *Hydrocarbon Processing,* 55, 1976, 153-158.

Koeppe, W., **On the Inversion Curve at Low Temperatures and Theorem of Corresponding States,** Proceedings of 10th International Congress on Refrigeration (Copenhagen 1959), Vol. 1, New York (1960), 156-163.

Llaguno, C.T., Sanchez, E.A.C., paper presented at the 1989 Meeting of the Philippine National Academy of Science and Technology.

Laurence, L.L., **Curves give temperature drop for expanding gases,** *WORLD OIL,* January 1984, 151-154.

Michelsen, M.L., **The Isothermal Flash Problem. Part I. Stability,** *Fluid Phase Equilibria,* 9 (1982) 1-19.

Miller, D.G., **Joule-Thomson Inversion Curve, Corresponding States, and Simpler Equations of State,** *Ind. Eng. Chem. Fundam.*, Vol.9, No.4, 1970, 585-589.

Montel, Elf Aquitaine, Private communication, 1994.

Nagy, S., **The influence of hydrocarbon condensation on natural gas throttling temperature,** *Archiwum Termodynamiki,* Vol.12 (1991) No 1-4, 101-115.

Pedersen, K.S., Thomassen, P., Fredenslund, Aa., **Characterization of Gas Condensate Mixtures,** Paper presented at the 1988 AIChE Spring National Meeting New Orleans, Louisiana, MArch 6-10, 1988.

Pedersen, K.S., Fredenslund, Aa., Thomassen, P., **Properties of Oils and Natural Gases,** Gulf Publishing Company, Houston, USA (1989).

Pitzer, K., Brewer,L., revisers, **Lewis and Randall's Thermoynamics,** Appendix 1, p. 611, McGraw-Hill, New York, 1961.

Randelman, R.E., Wenzel, L.A., **Joule-Thomson of Hydrogen and Methane Mixtures,** *J. Chem. Eng. Data,* **1988,** 33, 293-299.

Riazi, M.R., Daubert, T.E., **Simplify Propertiy Predictions,** *Hydrocarbon Processing,* Vol.59, 1980, 115-116.

Roebruck, J.R,, **The Joule-Thomson Effect in Air,** *Proceedings of the American Academy of Arts and Science,* Vol.64, No.13, 1925.

Roebuck, J.R., Osterberg,H., **The Joule-Thomson Effect in Nitrogen,** *Physical Review,* 48 (1935), 450.

Roebuck, J.R.,Murrell, T.A., Miller, E.E. **The Joule-Thomson Effect in Carbon Dioxide,** *J. Am. Chem. Soc.*, 64 (1942), 400-411.

Sage, B.H., Botkin, D.F., Lacey, W.N., **Joule-Thomson Coefficients for Two Natural Gases**, *Amer. Inst. of Mining & Metallugical Engineering*, Tech. Pub. No. 1504, *Petroleum Technology*, (Sept. 1942).

Sage, B.H., Webster, Lacey, W.N., **Joule-Thomson Coefficient of Ethane**, *Ind. Eng. Chem.*, Vol.29, No.6, June 1937, 665.

Sage, B.H., Kennedy, E.R., Lacey, W.N., **Joule-Thomson Coefficient of Propane**, *Ind. Eng. Chem.*, Vol.28, No.5, May 1936, 601-604.

Sim, W.J., Duabert, T.E., **Prediction of Vapor-Liquid Equilibria of Undefined Mixtures**, *Ind. Eng. Chem. Process Des. Dev.*, Vol.19, 1980, 386-393.

Ullmann's Encyclopedia of Industrial Chemistry, Verlag Chemie, 5th ed., Weinheim, 1985, Vol.B Unit Operations II, 20-6.

Wark, K., **Thermodynamics**, McGraw-Hill, New York, USA (1988), 5th ed., 512-515.

Winn, F.W., **Physical Properties by Nomogram**, *Petroleum Refiner*, Vol.36, 1957, 157-159.

Zemanski, M.W, Dittman, R.H., **Heat and Thermodynamics**, Sixth Edition, McGraw-Hill, Singapore (1981).

Appendices

Appendix A: Joule-Thomson Coefficient Formulas
Appendix B: Equations of State
Appendix C: Temperature Drop for Expanding Gases
Appendix D: Compositions of Gas-Condensate Mixtures

Table II. C_P **and** μ **for the VDW EOS by ADDS**

$C = RT_C/8$
$B = C/P_C$
$A = C(27B)$
$V_1 = RT$
$V_2 = V - B$
$V_3 = V_1/V_2$
$V_4 = V_3/(2A/V^3 - V_3/V_2)$
$C_P = C_P^{id} - RV_4/V_2$ **- R**
$\mu = -(V + V_4)/C_P$

Table III. C_P **and** μ **for the VIR EOS by ADDS**

$V_1 = B_3T$
$V_2 = B_2 + V_1$
$V_3 = B_1 + TV_2$
$V_4 = V_1 + V_2$
$B = B_0 + TV_3$
$V_5 = C_3T$
$V_6 = C_2 + V_5$
$V_7 = C_1 + TV_6$
$V_8 = V_5 + V_6$
$C = C_0 + TV_7$
$V_9 = C/V$
$V_{10} = B + V_9$
$V_{11} = V + V_{10}$
$V_{12} = V_{11} + T((V_3 + TV_4) + (V_7 + TV_8)/V)$
$V_{13} = V_{12}/(V_9 + V_{10} + V_{11})$
$V_{14} = 3T$
$C_P = C_P^{id} - R + R/V(V_{12}V_{13} - T(2(B_1 + V_4V_{14}) + (C_1 + V_8V_{14})/V))$
$\mu = (V_{13}V - V)/C_P$

Table IV. C_P **and** μ **for the BWR EOS by ADDS**

$V_0 = 2A\alpha$
$V_1 = B_0 + V$
$V_2 = RT$
$V_3 = T^2$
$V_4 = C_0/V_3$
$V_5 = V^2$
$V_6 = 1.0/(VV_5)$
$V_7 = \gamma/V_5$
$V_8 = 1 + V_7$
$V_9 = C \exp(-V_7)$
$V_{10} = V_9/V_3$
$V_{11} = 2(C_0V - V_9V_8)/V_3/T + R(B + V_1V)$
$V_{12} = TV_{11}/(V_2V + 2(A_0 - V_1V_2 + V_4 + (V_7^2V_{10} - 1.5(V_0V_6 - A + V_2B + V_8V_{10}))/V))$
$C_P = C_P^{id} - R + 3[V_{10}(2 + V_7)/(T\gamma) + .2(V_4/V - C/(\gamma V_5))/T] - V_{11}V_6V_{12}$
$\mu = -(V + V_{12})/C_P$

Table V. C_P **and** μ **for the RK EOS by ADDS**

$C_1 = RT_C$
$C_2 = C_1/P_C$
$A = 0.42748C_2C_1T_C^{1/2}$
$B = 0.08664C_2$
$C = 0.75A/B$
$V_1 = V - B$
$V_2 = R/V_1$
$V_3 = V + B$
$V_4 = TT^{1/2}$
$V_5 = A/(VV_3V_4)$
$V_6 = 0.5V_5 + V_2$
$V_7 = V_6/(V_5/V_3 + V_5/V - V_2/V_1)$
$C_P = C \log (V_3/V)/V_4 - V_6V_7 + C_P^{id} - R$
$\mu = -(V + V_7)/C_P$

Table VI. C_P **and** μ **for the SRK EOS by ADDS**

$C_1 = RT_C$
$C_2 = C_1/P_C$
$C_3 = T_C^{1/2}$
$C_4 = 0.48 + (1.57 - 0.176\omega)\omega$
$A = 0.42748C_1C_2$
$B = 0.08664C_2$
$C = AC_4(1 + C_4)/(2BC_3)$
$V_1 = T^{1/2}$
$V_2 = 1 + C_4(1 - V_1/C_3)$
$V_3 = V - B$
$V_4 = A/V$
$V_5 = V + B$
$V_6 = V_4/V_5$
$V_7 = R/V_3$
$V_8 = V_7 + (C_4/C_3)V_6V_2/V_1$
$V_9 = TV_8/(V_2V_2/V_5(V_6 + V_4/V) - T\ V_7/V_3)$
$C_P = C \log (V_5/V)/V_1 - V_8V_9 + C_P^{id} - R$
$\mu = -(V + V_9)/C_P$

Van der Waals

$$P = \frac{RT}{V-b} - \frac{a}{V^2} \qquad \textbf{(B.1)}$$

where : $a = \frac{27}{64}\frac{R^2T_c^2}{P_c}$ $b = \frac{1}{8}\frac{RT_c}{P_c}$ $Z_c = \frac{P_cV_c}{RT_c} = \frac{3}{8}$

Dieterici

$$P = \frac{RT}{V-b}\, e^{-a/RTV} \qquad \textbf{(B.2)}$$

where : $a = 4\frac{R^2T_c^2}{e^2}$ $b = \frac{RT_c}{e^2P_c}$ $e = 2.718$

Berthelot

$$P = \frac{RT}{V-b} - \frac{a}{TV^2} \qquad \textbf{(B.3)}$$

where : $a = \frac{27}{64}\frac{R^2T_c^3}{P_c}$ $b = \frac{9}{128}\frac{RT_c}{P_c}$

Redlich-Kwong

$$P = \frac{RT}{v-b} - \frac{a}{T^{0.5}v(v+b)} \qquad \textbf{(B.4)}$$

where : $a = 0.4275\frac{R^2T_c^{2.5}}{P_c}$ $b = 0.0867\frac{RT_c}{P_c}$

modified Redlich-Kwong

$$P = \frac{RT}{v-b} - \frac{a}{T^pv(v+qb)} \qquad \textbf{(B.5)}$$

where : $p = q = \frac{2}{3}$ $a = \frac{27}{64}\frac{R^2 T_c^{8/3}}{P_c}$ $b = \frac{3}{40}\frac{RT_c}{P_c}$

Soave-Redlich-Kwong

$$P = \frac{RT}{V-b} - \frac{a(T)}{V(V-b)} \qquad \textbf{(B.6)}$$

where : $a = 0.42747\frac{R^2 T_c^2}{P_c}\alpha(T_r,\omega)$ $b = 0.0867\frac{RT_c}{P_c}$

$$[\alpha(T_r,\omega)]^{1/2} = 1 + m(1 - T_r^{1/2})$$

$$m = 0.480 + 1.57\omega - 0.176\omega^2$$

Peng-Robinson

$$P = \frac{RT}{V-b} - \frac{a(T)}{V(V+b)+b(V-b)} \qquad \textbf{(B.7)}$$

where : $a = 0.45724\frac{R^2 T_c^2}{P_c}\alpha(T_r,\omega)$ $b = 0.07880\frac{RT_c}{P_c}$

$$[\alpha(T_r,\omega)]^{1/2} = 1 + m(1 - T_r^{1/2})$$

$$m = 0.37464 + 1.54226\,\omega - 0.26992\,\omega^2$$

Lee-Kesler

$$Z = Z^{(0)} + \frac{\omega}{\omega^{(r)}}[Z^{(r)} - Z^{(0)}] \qquad \textbf{(B.8)}$$

$Z^{(0)}$ and $Z^{(r)}$ are given by the Benedict-Webb-Rubin (BWR) equation, with constants fitted to simple fluid behaviour for $Z^{(0)}$ and to n-octane data for $Z^{(r)}$:

$$Z = \frac{p_r V_r}{T_r} = 1 + \frac{B}{V_r} + \frac{C}{V_r^2} + \frac{D}{V_r^5} + \left(\frac{c_4}{T_r^3 V_r^2}\right)\left(\beta + \frac{\gamma}{V_r^2}\right)e^{(-\gamma/V_2^2)} \qquad \textbf{(B.9)}$$

where B, C and D are functions of the reduced temperature

$$B = b_1 - \frac{b_2}{T_r} - \frac{b_3}{T_r^2} - \frac{b_4}{T_r^3}$$

$$C = c_1 - \frac{c_2}{T_r} - \frac{c_3}{T_r^3}$$

$$D = d_1 - \frac{d_2}{T_r}$$

Lee and Kesler presented tables of the 12 constants b_i, c_i, d_i, β and γ for the simple fluid and for the reference fluid.

GEoS

$$P = \frac{RT}{v-b} - \frac{a(T)}{(v-d)^2 + c} \qquad \textbf{(B.10)}$$

By setting the four critical conditions for T_r=V_r=1,

$$P_r = 1 \qquad \frac{\partial P_r}{\partial V_r} = 0 \qquad \frac{\partial^2 P_r}{\partial V_r^2} = 0 \qquad \frac{\partial P_r}{\partial T_r} = \alpha_c$$

for the reduced form,

$$P_r = \frac{T_r}{U + B} - \frac{A\beta(T_r)}{(U + D)^2 + C} \qquad \textbf{(B.11)}$$

where

$$U = Z_c(V_r - 1) \qquad \textbf{(B.12)}$$

one finds:

$$A = (1 - B)^3 \quad ; \quad B = (1 + m)/(\alpha_c + m)$$

$$C = (1 - B)^2(B - 0{,}25) \quad ; \quad D = (1 - B)/2$$

where m is used as an adjustable parameter in the $\beta(T_r)$ function, as well as Riedel's criterion α_c. Values of m and α_c parameters of the GEoS used for calculation are given in table B.1.

Table B.1 Values of m and α_c parameters of the GEoS

Component	$\beta_1(T_r)$		$\beta_2(T_r)$	
	m	α_c	m	α_c
Ar	0.1612	5.8818	0.2140	6.0860
CO_2	0.3468	7.056	0.3860	7.3150

TABLE 1—Molecular weight of various natural gases

	Molecular weight												
	16	16.9	17.6	18.5	19.1	21.7	24.1	25.2	25.7	29.5	35.5	41.4	42.4
	Component, Mol. %												
CO_2	–	0.5	0.99	1.20	0	0.50	0.65	0.794	0.90	0	0	0	0.13
H_2	–	0	0	0	0	0	0.47	1.375	0	0	0	0	0.76
C_1	100	96.28	93.56	90.89	94.11	86.3	86.59	76.432	78.05	60.0	44.0	59.7	53.91
C_2	–	2.0	3.37	4.40	2.67	5.0	3.76	7.923	7.42	15.0	20.0	8.9	14.20
C_3	–	0.70	1.08	1.91	0.89	3.0	1.61	4.301	4.88	10.0	15.0	5.0	9.64
IC_4	–	0.10	0.20	0.33	0.21	0.8	0.48	1.198	1.18	4.0	5.0	2.9	1.25
NC_4	–	0.20	0.40	0.60	0.34	0.8	0.82	1.862	1.65	4.0	5.0	2.0	4.29
IC_5	–	0.07	0.15	0.21	0.20	0.6	0.44	0.937	0.75	2.0	3.0	5.0	1.12
NC_5	–	0.07	0.10	0.13	0.10	0.6	0.22	0.781	0.60	2.0	3.0	4.3	1.87
C_6	–	0.05	0.10	0.15	0.29	0.9	0.62	1.405	1.04	–	–	–	2.72
C_7	–	–	–	–	–	0.5	1.00	0.585	–	–	–	–	–
C_8	–	–	–	–	–	–	–	1.040	0.923	3.0	5.0	–	–
C_9	–	–	–	–	–	–	–	0.613	0.843	–	–	–	–
C_{10}	–	–	–	–	–	–	–	0.338	0.712	–	–	12.2	–
C_{11}	–	–	–	–	–	–	3.34	0.176	0.570	–	–	–	–
C_{12}	–	0.03	0.05	0.18	1.19	1.0	–	0.153	0.482	–	–	–	10.11
C_{13}	–	–	–	–	–	–	–	0.087	–	–	–	–	–
Total	100	100.00	100.00	100.00	100.00	100.0	100.0	100.000	100.000	100.0	100.0	100.0	100.00

TABLE 2—Molecular weight vs. temperature change (°F)

	Expansion from 10,000 to 5,000 psig Temperature change, °F												
Molecular weight	16	16.9	17.6	18.5	19.1	21.7	24.1	25.2	25.7	29.5	35.7	41.4	42.4
10,000 psig	0	0	0	0	0	0	0	0	0	0	0	0	0
9,500	+1	+1	+1	+1	+2	+2	+2	+2	+2	+2	+3	+3	+4
9,000	+2	+2	+2	+2	+3	+3	+4	+4	+4	+5	+6	+7	+7
8,500	+3	+3	+3	+3	+4	+5	+6	+6	+6	+7	+9	+10	+10
8,000	+3	+4	+3	+4	+5	+6	+8	+8	+8	+10	+12	+13	+14
7,500	+3	+4	+4	+4	+6	+7	+10	+9	+10	+13	+15	+17	+17
7,000	+3	+4	+3	+4	+6	+8	+11	+11	+11	+14	+18	+20	+20
6,500	+3	+3	+3	+3	+6	+8	+12	+12	+12	+16	+20	+23	+23
6,000	+1	+2	+2	+2	+5	+8	+12	+12	+13	+17	+23	+26	+26
5,500	0	0	0	+1	+4	+7	+12	+13	+13	+18	+25	+28	+29
5,000	−3	−2	−1	−1	+2	+6	+12	+12	+13	+19	+27	+31	+32
	Expansion from 5,000 to 0 psig Temperature change, °F												
5,000 psig	0	0	0	0	0	0	0	0	0	0	0	0	0
4,500	−3	−3	−4	−4	−2	−2	−1	−1	−1	+1	+2	+2	+2
4,000	−7	−8	−9	−8	−6	−5	−4	−3	−2	+1	+4	+4	+5
3,500	−13	−13	−15	−14	−11	−10	−7	−6	−5	0	+5	+6	+7
3,000	−21	−21	−22	−21	−18	−16	−13	−8	−9	−2	+6	+8	+8
2,500	−30	−31	−32	−31	−26	−25	−20	−17	−17	−6	+6	+8	+9
2,000	−43	−44	−45	−45	−38	−37	−29	−27	−27	−10	+5	+6	+7
1,500	−59	−61	−63	−63	−54	−52	−42	−41	−40	−21	+4	0	0
1,000	−81	−84	−87	−87	−74	−72	−59	−59	−58	−39	−9	−12	−12
800	−91	−97	−99	−98	−88	−82	−73	−72	−67	−48	−17	−18	−18
600	−103	−108	−112	−111	−100	−92	−83	−80	−77	−59	−27	−24	−26
400	−116	−121	−126	−125	−112	−105	−94	−91	−89	−73	−41	−33	−36
200	−130	−136	−142	−142	−127	−121	−110	−108	−105	−94	−62	−45	−52
ATMS	−145	−153	−160	−163	−147	−155	−125	−150	−146	−163	−134	−87	−101

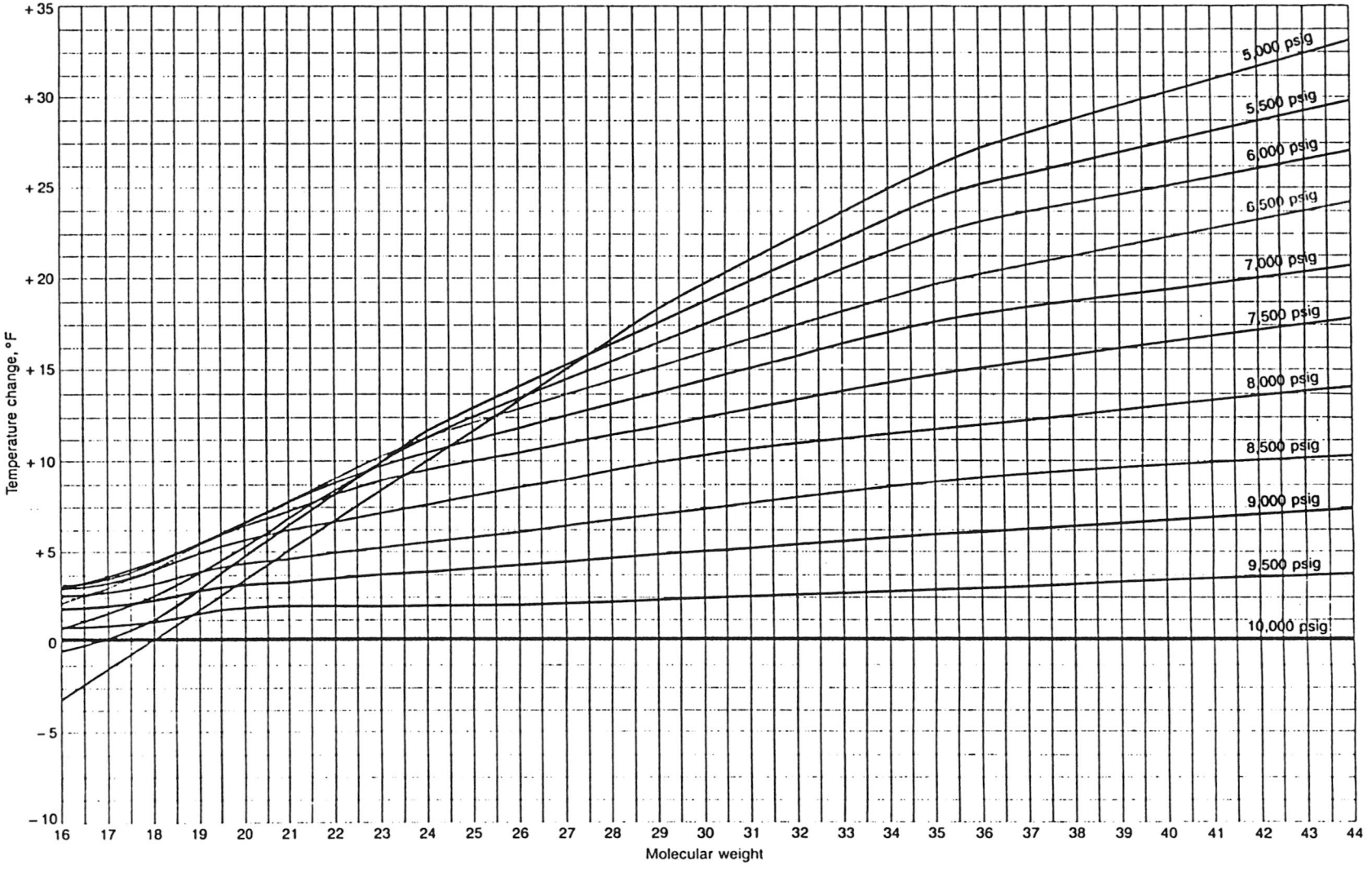

Fig. 1—Adiabatic expansion from 10,000 to 5,000 psig.

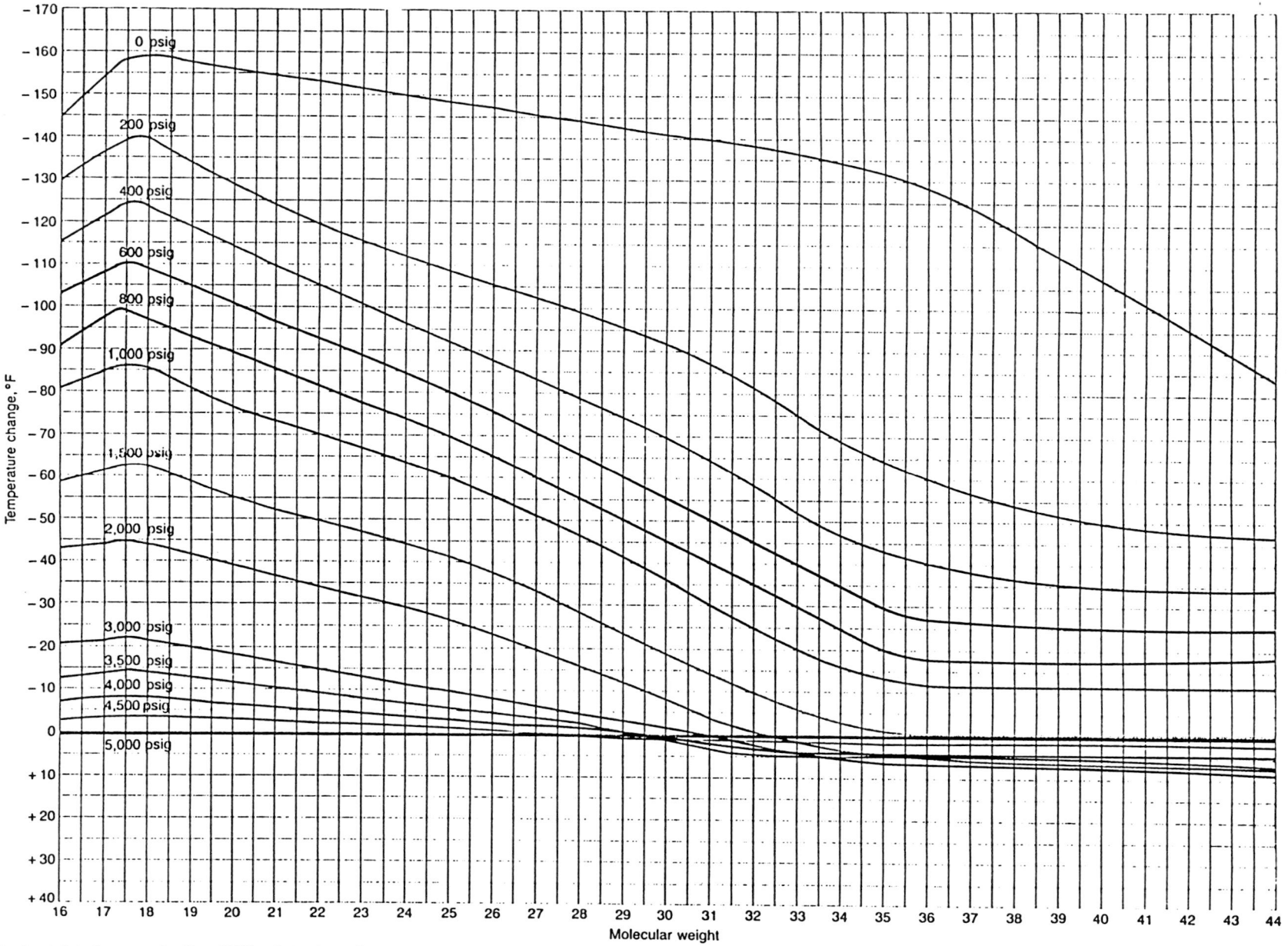

Fig. 2—Adiabatic expansion from 5,000 psig to atmosphere.

Table D.1 Varaiations in compostions of gas-condensate mixtures

Component	mixture 1 †	mixture 2 ‡	mixture 3 †	mixture 4 #	mixture 5 ‡	mixture 6 †	mixture 7 ‡	Montel \	Montel \
N_2	0.71	-	0.85	0.23	0.12	0.46	0.64	0.554	0.255
CO_2	8.64	-	0.65	2.12	2.49	3.36	9.16	2.619	3.598
C_1	70.85	91.34	83.58	73.15	76.43	62.23	68.80	68.444	74.117
C_2	8.53	4.03	5.95	9.39	7.46	8.88	8.43	8.981	7.944
C_3	4.95	1.53	2.91	4.86	3.12	5.30	5.11	4.240	3.294
n-C_4	1.26	0.43	1.11	1.78	1.21	2.07	1.45	1.517	1.242
i-C_4	0.75	0.39	0.45	1.02	0.59	0.91	0.81	0.801	0.680
n-C_5	0.40	0.19	0.48	0.49	0.59	0.85	0.53	0.658	0.608
i-C_5	0.41	0.15	0.36	0.60	0.50	0.73	0.52	0.676	0.552
C_6	0.46	0.39	0.60	0.93	0.79	1.04	0.63	1.390	0.874
C_7	0.61	0.361	0.80	5.43	0.95	1.84	0.83	1.707	1.147
C_8	0.71	0.285	0.76		1.08	1.73	0.95	1.495	1.072
C_9	0.39	0.222	0.47		0.78	1.39	0.52	1.121	0.748
C_{10}	1.33	0.672	1.03		0.592	9.21	0.26	0.912	0.565
C_{11}					0.467		0.20	4.884	3.302
C_{12}					0.345		0.17		
C_{13}					0.375		0.16		
C_{14}					0.304		0.15		
C_{15}					0.237		0.11		
C_{16}					0.208		0.086		
C_{17}					0.220		0.078		
C_{18}					0.169		0.068		
C_{19}					0.140		0.050		
C_{20}					0.833		0.284		

† Pedersen et al. (1988)
‡ Pedersen et al. (1989)
# Aasberg-Petersen and Stenby (1991)
\ Montel (1994)